Anatomical Differences across Cerebellar Neuronal Networks in Valproic Acid (VPA) Induced Rats

Lila Haleblian

A Thesis
In the Department
Of
Health, Kinesiology and
Applied Physiology

Presentation in Partial Fulfilment of the Requirements
For the Degree of Master of Science (Health and Exercise Science) at
Concordia University
Montreal, Québec, Canada

March 2023

CONCORDIA UNIVERSITY

School of Graduate Studies

This is to certify that the thesis prepared

By: Lila Haleblian

Entitled: Anatomical Differences across Cerebellar Neuronal Networks in Valproic Acid (VPA) Induced Rats

and submitted in partial fulfillment of the requirements for the degree of

Master of Science (Health and Exercise Science)

complies with the regulations of the University and meets the accepted standards with respect to originality and quality.

Signed by the final examining committee:

_____ Chair of Defense

Dr. Geoffrey Dover

_____ Examiner

Dr. Shimon Amir

_____ Examiner

Dr. Christopher Steele

_____ Internal to Program Examiner

Dr. Nancy St-Onge

_____Thesis Supervisor

Dr. Richard Courtemanche

Approved by _____

Dr. Geoffrey Dover, Graduate Program Director, HKAP

_____

Dr. Pascale Sicotte, Dean of the Faculty of Arts and Science

ABSTRACT

Anatomical Differences across Cerebellar Neuronal Networks in Valproic Acid (VPA) Induced Rats

Lila Haleblian
Concordia University, 2023

The cortico-cerebellar circuits are highly involved in the coordination of sensorimotor processes and are crucial for the expression of sensorimotor and, with more recent literature, cognitively demanding behaviors in early childhood. Through these circuits, cerebellar differences could impact behavioral changes characterized in many neurological disorders, including Autism Spectrum Disorder (ASD). Despite the increasing prevalence of the disorder, insights into the anatomical differences across cerebellar neuronal networks in ASD remain poorly understood. The objective of this thesis is to characterize the cerebellar circuitry in a valproic acid (VPA)-induced animal model of ASD. Tissues were stained with Cresyl violet and captured with a confocal microscope. First, we examined the counts in (1) Purkinje cell (PC) and (2) Deep cerebellar nuclei (DCN) cells while measuring their density. Consistent with our hypothesis, we found that there were: (1) significant losses in PC density in the posterior inferior regions of lobules Crus I, Crus II, PM, and Cop of the hemisphere, and (2) significantly higher DCN density of the medial nuclei, contrary to our hypothesis, in the VPA-exposed rats compared to the control. Then, we examined the granule cell layer (GCL) thickness measurements across the lobules of the vermis and hemisphere and found that GCL thickness of Lobule 6 was lower, while Lobule 7-8-9 and Lobule 10 were higher in the VPA-exposed rats compared to control. Finally, we found a correlation and cross-covariance between the PC and GCL thickness measurements in the lobules of the posterior lobe. These findings suggest alterations in cerebellar anatomy affected by the VPA, and therefore further support the implication of the cerebellum and cerebellar circuits in VPA-exposed rats.

ACKNOWLEDGEMENT

First, I would like to take this opportunity to express my utmost gratitude to my supervisor, Dr. Richard Courtemanche. Two years ago, when COVID-19 started, I had just graduated from my Bachelor's in Biology and was uncertain about my academic and professional aspirations. One thing I knew for certain was that I was deeply interested in Human Sciences although I lacked the hands-on experience in the field. Despite these issues, you offered me the invaluable opportunity to join your lab as a graduate student and have been astounded by your extensive knowledge of the field of neuroscience and physiology. Over the past three years, I have been continuously impressed by your dedication to learning and am humbled and grateful for your constant guidance and trust in me. As a student, it is important to have a supervisor who cares and is there every step of the way. Without your mentorship, I cannot imagine where or how I would have achieved my current academic goals. I am deeply grateful for this experience. Once again, thank you for everything.

Second, I would like to thank Dr. Shimon Amir and Dr. Sarah Ferraro, for helping me pursue this great project, and for all the help that you have offered me throughout my project. A large part of this achievement is because of your generosity and help. I would also like to extend my thanks to Chris Law for showing me how to use the microscope from the Centre for Microscopy and Cellular Imaging (CMCI) and being patient and willing to help when needed.

Finally, I would like to express my sincerest gratitude to my beloved family and friends for their unwavering support and affection. To my mom, Maria, who has taught me to never give up on what I believe in. I am the person I am today because of all the sacrifices and hard work that you have made throughout your life. To my brothers, Edy and Alex, your unwavering support and presence have been a source of immense strength for me. Even amidst a captivating soccer match, you have stood by me. To my two cherished friends, Gaëlle and Cristen, life would not be the same without you. Lastly, I would like to express my heartfelt appreciation to my partner, Karim, for his boundless encouragement, devotion, and endurance over the past few years. Your influence has significantly impacted my life and has been an integral part of my journey. Thank you all.

Table of Contents

List of Figures

List of Tables

List of Abbreviations

ANOVA: Analysis of Variance

ASD: Autism Spectrum Disorder

CF: Climbing fiber

CMIC: Centre for Microscopy and Cellular Imaging

CN: Cerebellar nuclei

COP: Copula pyramidis

CPC: Cortico-ponto-cerebellar

CTC: Cerebello-thalamo-cortical

DCN: Deep cerebellar nuclei

DTI: Diffusion tensor imaging

FA: Fractional anisotropy

fMRI: Functional magnetic resonance imaging

GCL: Granule cell layer

GD: Gestational day

HDAC: Histone deacetylase inhibitor

ICP: Inferior cerebellar peduncle

MCP: Middle cerebellar peduncle

MD: Mean diffusivity

MRI: Magnetic resonance imaging

PF: Parallel fiber

PND: Post-natal day

PBS: Phosphate saline solution

PC: Purkinje cell

PM: Paramedian lobule

PN: Pontine nuclei

SAL: Saline

SCP: Superior cerebellar peduncle

SEM: Standard error of means

VPA: Valproic acid

ZT: Zeitgeber Time

Introduction

Brain Connectivity & Architecture

Interconnected parts of the brain coordinate to process sensorimotor and cognitive information. The neurophysiology of circuit communication across multiple brain regions such as the cerebral cortex, the cerebellum, and the basal ganglia ensures optimality in cognitive and sensorimotor processes that are essential for survival. Essentially, our cognitive and motor behaviors (e.g., thought, planning and locomotion) are expressed through the coordinated neural communication of large populations of interconnected neurons across different brain areas (Gray, 1994). These functional ensembles operate through a process of signaling that is the outcome of a series of operations conducted at the levels of membranes, molecules, and ion channels, all of which are ultimately encoded by genes (Figure 1). This hierarchy of levels in the brain: from detailed molecular-level genes, by way of neuronal cells, to the entire neuronal networks generating behavior; these relationships remain only partially understood. To improve the understanding of mechanisms that subtend physiological and pathological dynamics, these "connectome" networks are usually investigated at three different levels: the *macroscale* which focuses on inter-areal connections, the *mesoscale* which addresses connections at the cellular level (between neuronal types across different brain regions), and the *microscale*, which tackles connections between individual neurons at the synaptic and subsynaptic levels (Zeng, 2018; Palesi et al. 2020).

At the microscale connectome level, neurons and their dendritic and axonal projections form local neuronal microcircuits, which constitute the basic elements of brain architecture. Many studies have investigated the importance of neuronal features such as dendritic tree length, number of dendritic branches, and/or spine density and the functional adaptations they represent across cells from different brain regions. Such features are proven to be directly linked to a region's communication and information processing efficiency (Heuvel and Yeo, 2017). The combination of single-neuron scans to image local networks results in a mesoscale connectome comprising of multiple nodes and their weighted interconnections (Sporns, 2016). A common feature of mesoscale structure is modularity, which measures the strength of subdivision of a network into a module. Mesoscale network architecture is a defining feature in the understanding of the structural organization of the brain and its functions (Khambhati et al. 2018). In turn, the integration of such microstructures and networks results in the large-scale circuit description: the macroscale connectome. At the macroscale level, the network connectivity across cortical regions is based on the anatomical complexity and functional diversity of larger population dynamics. One example of large-scale functional network through which multiple brain regions communicate to process sensorimotor information consists in the cerebro-ponto-cerebellar and cerebello-thalamo-cortical loops. These networks feature route-specific information between parts of the brain dedicated to motor planning and control. In fact, different types of neurons in the cerebral cortex are selectively stimulated by and ensure the functional interconnection between different structures depending on stimulus features they must encode (Spaeth et al. 2022; D'Mello and Stoodley, 2015). This level of specificity and precision at the neuronal level highlights the significance of understanding brain connectivity and network organization at the microscale, mesoscale and macroscale connectome levels.

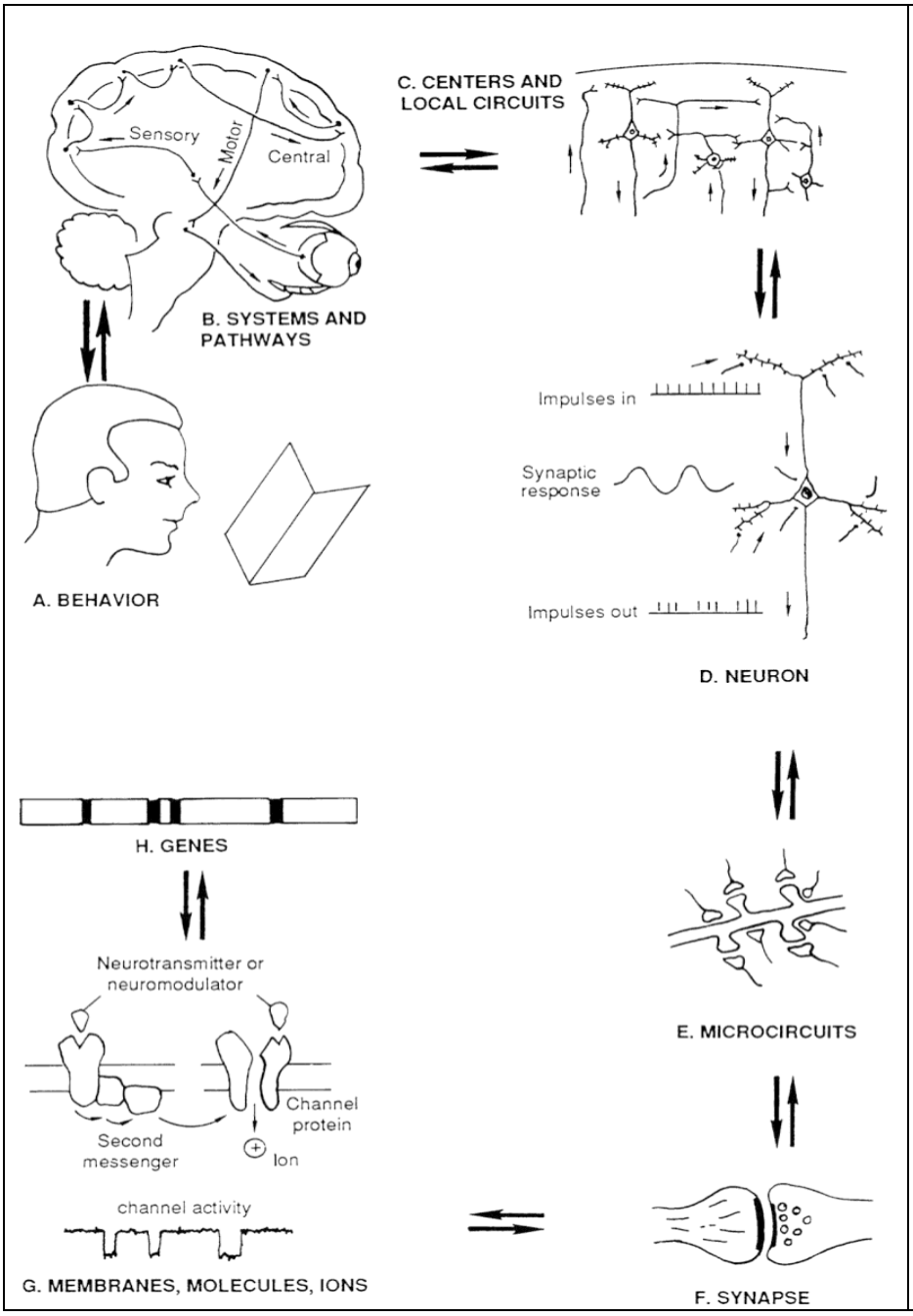

Figure 1: Level of organization in the central nervous system. The relations between the different levels are bidirectional. Scientific inquiry can consider different related levels, including the start at the genetic (G) or the behavioral level (A), or in intermediate levels. From genes (H), and proteins that are encoded by genes at the membrane level (G), successively building up to higher levels of molecular signaling pathways through synapses (F), microcircuits (E), neurons (D), centers and local circuits (C), and specific neuronal pathways and systems (B) to coordinated output of those systems that generate behavior (A) (Shepherd, 1994).

Cerebro-cerebellar Circuits and Cerebellar Topography

Earlier cerebellar research has focused primarily on cerebellum's role in balance, posture, and motor control; however, emerging evidence is mounting that the cerebellum is implicated in cognitive and affective information processing as well. Quantitatively, its neuronal counts are a bit surprising yet evocative of its importance: the cerebellum covers 10% of the brain's volume yet contains over half of all the neurons in the brain (Herculano-Houzel, 2010). A substantial portion of the cerebellum forms reciprocal, closed-loop circuits with the cerebral cortex and subcortical structures associated with non-motor functions including attention and working memory (Brissenden et al. 2018). Because of this closed-loop organization and uniform circuitry, a prevailing hypothesis is that the cerebellum contains parallel processing modules, the function of which is driven by the input the module receives. Therefore, functional subregions of the cerebellum interact with specific regions of the cerebral cortex, forming particular processing channels. Although not separated definitely and showing some overlap, the anterior lobe region of the cerebellum is structurally and functionally connected to sensorimotor areas of the cerebral cortex, while the posterior lobe region of the cerebellum is structurally and functionally more connected to cognitive regions, including prefrontal, and parietal association cortices (O'Reilly et al. 2010).

As hinted above, in sensorimotor and cognitive processing (at least), the cerebellum engages in close communication with the cerebral cortex through two main pathways: the efferent cerebello-thalamo-cortical (CTC) pathway and the afferent cortico-ponto-cerebellar (CPC) pathway [see Figure 2, for a schematic illustration of these loops in the human brain] (Palesi et al. 2017). On the one hand, the CTC pathway originates from the cerebellum, passes through the superior cerebellar peduncle (SCP), and reaches the motor cortex by way of the relay of the thalamus (Palesi et al. 2017). On the other hand, in the afferent CPC pathway, the cerebral cortex communicates with the cerebellum through monosynaptic projections to the pontine nuclei (PN); the information gets transmitted to the cerebellar cortex, through the PN mossy fibers, passing through the middle cerebellar peduncle (MCP) to finally reach the deep cerebellar nuclei (DCN) and the cerebellar cortex. In the latter instance, the mossy fibers will intersect with the granule cells and Golgi cells in the cerebellar cortex, moving across the layers, as granule cells will relay excitatory signals to the Purkinje cells, which in turn will send inhibitory signals to the DCN. As for the output of the cerebellum, the DCN project to the thalamus, which sends connections back to frontal lobe including its primary motor cortex, closing the cortico-cerebellar loop (Guo et al. 2021).

(A)

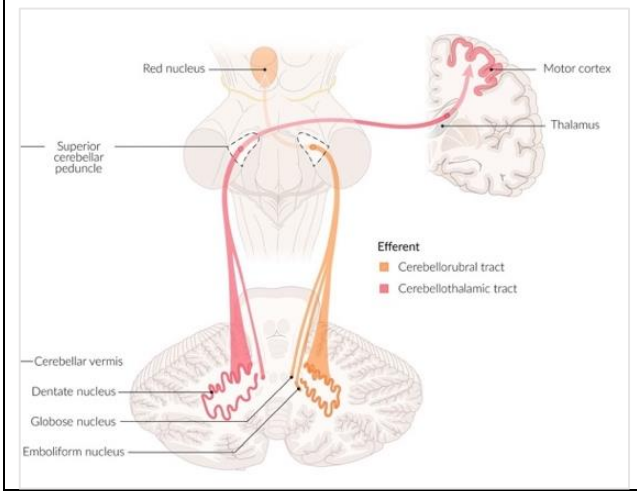
Red nucleus
Motor cortex
Thalamus
Superior cerebellar peduncle
Efferent
Cerebellorubral tract
Cerebellothalamic tract
Cerebellar vermis
Dentate nucleus
Globose nucleus
Emboliform nucleus

(B)

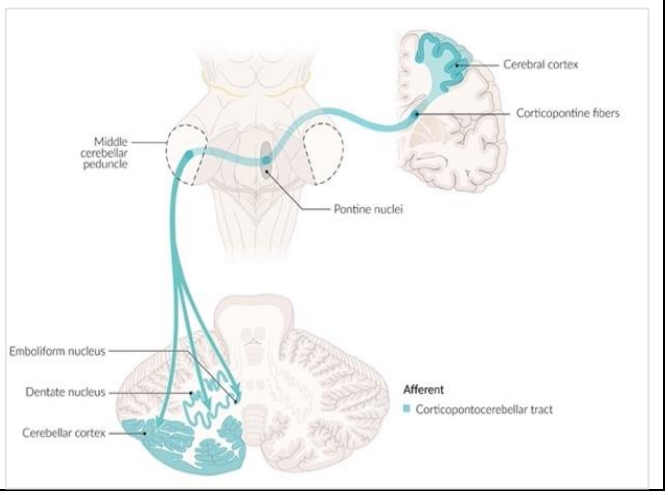
Cerebral cortex
Corticopontine fibers
Middle cerebellar peduncle
Pontine nuclei
Emboliform nucleus
Dentate nucleus
Cerebellar cortex
Afferent
Corticopontocerebellar tract

Figure 2: Representation of the human cerebro-cerebellar loops. (A) The cerebello-thalamo-cortical (CTC) tract is the output pathway of the cerebellum, where neural communication goes from the cerebellum, passes through the superior cerebellar peduncle, and reaches the frontal lobe and motor cortex through the thalamus (Picture taken from AMBOSS, USA, and verified with Palesi et al. 2017). (B) The cortico-ponto-cerebellar (CPC) tract is the input pathway to the cerebellum. In one direction, neural communication goes from the cerebral cortex, passes through the pontine nuclei and the middle cerebellar peduncle, and reaches all four deep cerebellar nuclei cells (emboliform, dentate, fastigial, and globose).

Cerebellar circuitry

Despite its dense packing of cells, the flow of information from and into the cerebellum appears to be functionally and structurally organized. For instance, the cerebellar cortex is comprised of three layers: the granule cell layer (GCL), Purkinje cell (PC) layer, and molecular layer (Figure 3A) where the cerebellar cortex cells are orderly arranged and receive extensive information from multiple parts of the brain through the mossy fiber inputs (Hampson and Blatt, 2015). One of the key neuronal types in the cerebellar circuitry and the unique output cells of the cerebellar cortex are known as the Purkinje cells (PCs). PCs play an important role in the coordination and regulation of the behavior and actions, and this neural population is decreased in numbers in Autism Spectrum Disorder (ASD). The Purkinje cells receive input from two distinct pathways: the olivocerebellar connections, and the axons coming from mossy-fiber granule cell excitatory afferents, the ascending axons and parallel fibers. The most voluminous source of input to the PCs comes from these afferents, whose source originates from various spinal cord, brainstem and pontine nuclei that relay information to the granule cells via the mossy fibers; input to the cerebellum also comes from the inferior olivary nuclei via the excitatory olivocerebellar climbing fibers (CFs) to the branches of PCs (Figure 3B). The axonal extensions of the granule cells, the parallel fibers (PFs), direct the signals to the branches of the PCs in the molecular layer (Figure 3B, Purves et al. 2001; Hampson and Blatt, 2015). Parallel fibers also connect with local circuit neurons, such as the basket and stellate cells, forming inhibitory loops with the PCs (Figure 3B, Purves et al. 2001).

Beyond the three layers of the cerebellar cortex, a dense network of white matter fiber tracts (input and output), we also find in the cerebellum the central nuclei, labelled collectively as DCN. These nuclei contain neurons that send the output information from the cerebellum (with the exception of the vestibular part of the cerebellum who send this to brainstem vestibular nuclei). Therefore, for the large majority of cerebellar operations, once the neural impulses reach the branches of the PCs and travel through the PC axons, they will modulate (increase or decrease their inhibition on) the DCN cells; in turn, these DCN cells send the signaling output to the thalamus (Figure 3B, Purves et al. 2001). Each nucleus is comprised of GABAergic, glycinergic, and glutamatergic cell types. In rodents, these nuclei are qualified by their anatomical position: medial, intermediate, and lateral (Figure 3C). In primates and humans, the nomenclature is different and based on historical anatomical descriptions and complexity: the medial nucleus is called fastigial, the intermediate is comprised of the distinct globose and emboliform nuclei (which together constitute the interposed nucleus), and the rodent lateral nucleus is replaced by the dentate, with a more complex, convoluted structure (Gill and Sillitoe, 2019). Together, the DCN represent the general link of the cerebellar cortex to the rest of the brain and spinal cord (Figure 3C). Therefore, in the cerebellum, excitation and inhibition interact at the level of the cortex and DCN, an important comparative process in the regulation of neural connectivity with multiple cerebral cortex regions. The optimality in information transmission through cerebro-cerebellar loops is essential for accurate and timely flow of information serving efficient brain operations; disturbance of these loops have proven to be a determinant of pathophysiological manifestations involved in several clinical conditions. The abnormal functioning of cerebro-cerebellar pathways likely subtends major neurological conditions such as ataxia, dystonia, essential tremor, hemiplegia, stroke, attention deficit hyperactivity disorder (ADHD) and ASD (Palesi et al. 2017).

(A)

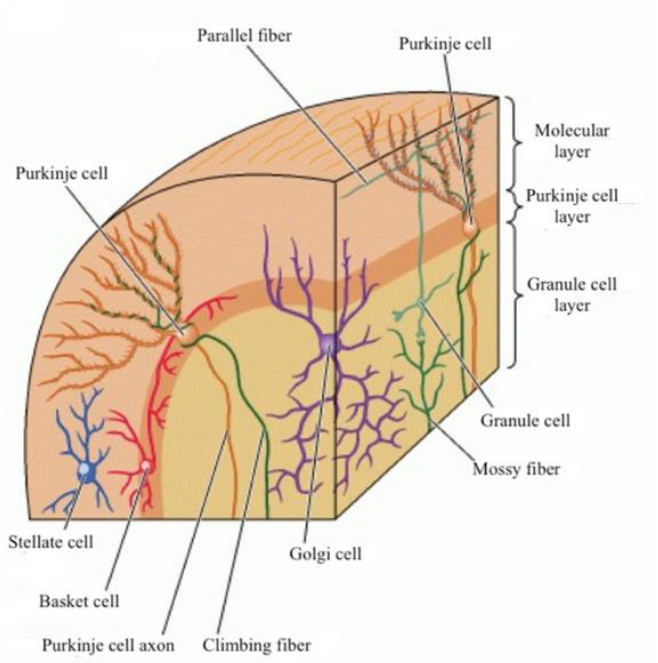
Parallel fiber
Purkinje cell
Purkinje cell
Molecular layer
Purkinje cell layer
Granule cell layer
Granule cell
Mossy fiber
Stellate cell
Golgi cell
Basket cell
Purkinje cell axon
Climbing fiber

(B)

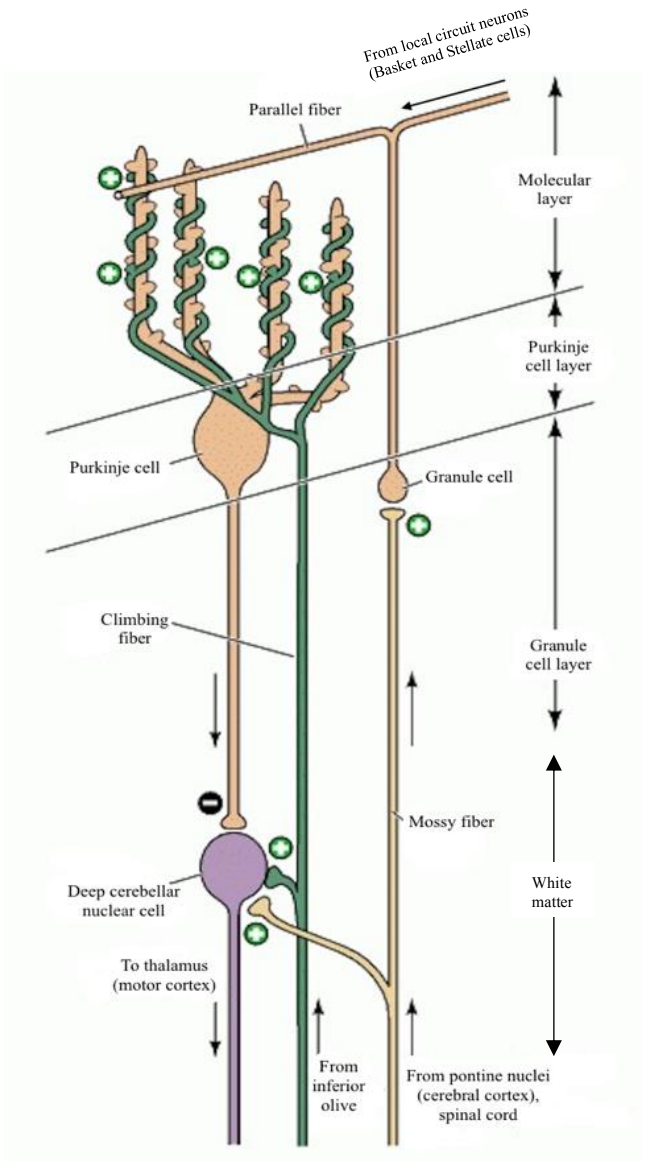
From local circuit neurons (Basket and Stellate cells)
Parallel fiber
Molecular layer
Purkinje cell layer
Purkinje cell
Granule cell
Climbing fiber
Granule cell layer
Mossy fiber
Deep cerebellar nuclear cell
White matter
To thalamus (motor cortex)
From inferior olive
From pontine nuclei (cerebral cortex), spinal cord

(C)

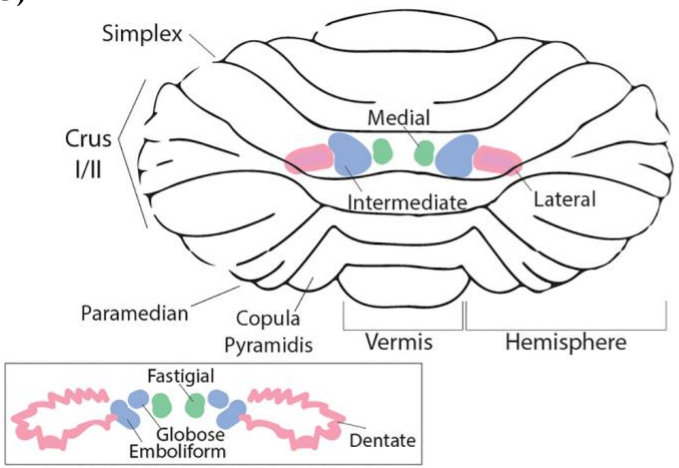
Simplex
Crus I/II
Medial
Intermediate
Lateral
Paramedian
Copula Pyramidis
Vermis
Hemisphere
Fastigial
Globose
Emboliform
Dentate

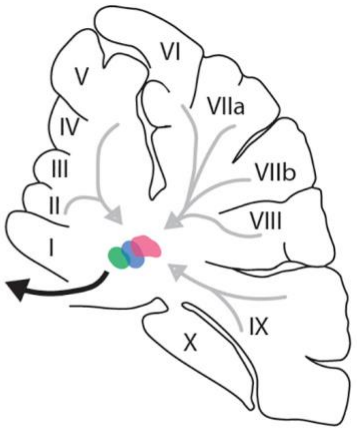
VI
V
VIIa
IV
III
VIIb
II
VIII
I
IX
X

Figure 3: Neurons and circuits of the cerebellum. (A) Neural organization of the cerebellar cortex in three distinct layers: molecular layer, Purkinje cell layer, and granule cell layer (Purves et al. 2001). (B) Excitatory and inhibitory connections in the cerebellar cortex and deep cerebellar nuclei. The excitatory input is received through mossy fibers and climbing fibers to Purkinje cells (PCs) to the deep cerebellar nuclear cells. Additional convergent input to the PCs is received from local circuit neurons (basket and stellate cells) through the parallel fibers. Golgi cells not indicated. The output from the cerebellum is through the axons of the PCs onto the deep cerebellar nuclear cells. The (+) and (-) signs represent the excitatory and inhibitory neurons, respectively (Purves et al. 2001). (C) Rodent cerebellum depicted from the dorsal view (left panel). Vermis is midline. The deep cerebellar nuclei (DCN) are represented in color; pink: lateral nucleus, green: medial nucleus, and blue: intermediate nucleus. Bottom inset, same for the primate cerebellar nuclei (CN). Dentate (lateral, pink), fastigial (medial, green), and globose and emboliform nuclei (blue), the latter two together forming the interposed nuclei. Right panel, representation of a parasagittal view of the cerebellum at midline. The CN are indicated, with light gray arrows representing schematized Purkinje cell output, and black arrow representing DCN efferent projections to the cerebral cortex and brainstem (Gill and Sillitoe, 2019).

Overview of ASD

Affecting an increasing number of people, ASD is a highly heritable and heterogeneous group of neurodevelopmental disorders that normally persist throughout life. The prevalence of ASD diagnosis ranges from 1.46% to 2.5% in children and is approximately four times more common in male compared to female individuals (Weston, 2019). According to the Diagnostic and Statistical Manual of Mental Disorders, ASD diagnosis is confirmed by deficits in motor control and cognitive functions (American Psychiatric Association, 2013). Some of the hallmark features expressed in ASD include impairments in social and communication skills that start to develop at an early age, and impairments in some basic motor control functions, with the expression of stereotyped movements (such as hand flapping and/or in repetitive speech), and affected bilateral coordination (Weston, 2019; Moore et al. 2000; Ozonoff et al. 2010).

Cerebro-Cerebellar Pathways Affected in ASD

There has been a long-ranging effort in linking impairments in motor coordination and social communication in patients with ASD with distinctive patterns of brain connectivity. Emerging research on structural and functional ASD patterns using magnetic resonance imaging (MRI and fMRI) have aimed to identify alterations in neural connectivity as a potential cause for behavioral alterations observed in ASD individuals (Minshew & Keller, 2010; Schumann & Nordahl, 2011). Recent studies report excessive short-range connectivity within cortical regions (such as the frontal and parietal cortices) in ASD as well as poor long-range connectivity between cortico-cortical structures (such as the frontal and occipital cortices) or cortico-subcortical structures, including the sensorimotor, premotor, and supplementary motor cortices with the cerebellum or basal ganglia (Kaur et al. 2018).

An analysis was conducted on fiber tracts within the cerebellum and its input and output pathways, utilizing diffusion tensor imaging (DTI) and tractography methods. Fractional anisotropy (FA) and mean diffusivity (MD) were collected to measure the overall directionality of water diffusion and the rotationally invariant magnitude of water diffusion within brain tissues, respectively (Clark et al. 2011). Typically, high FA levels indicate increased microstructural integrity or fiber organization, while decreased FA levels indicate reduced myelination, inflammation along the axon, and decreased fiber density (Clark et al. 2011). Conversely, high MD values reflect reduced numbers or packing of neural and glial cells (D'Mello and Stoodley, 2015). In individuals with autism spectrum disorder (ASD), D'Mello and Stoodley (2015) reported decreased FA and increased MD in the corpus callosum, cingulum, and white matter within the temporal and frontal lobes. These diffusion differences observed over the trajectory of certain pathways in ASD patients can lead to significant changes in brain connectivity (Pierpaoli et al. 2000).

Individuals with ASD show altered structural connectivity within the cerebellum and in the projection fibers carrying information to and from the cerebellum: the output and input pathways of the cerebellum also show difference in FA and MD in ASD patients. More specifically, the middle and inferior cerebellar peduncles (MCP and ICP) show FA and MD abnormalities affecting the relay of information to the cerebellum from the cerebral cortex and the spinal cord/inferior olive/vestibular nuclei, respectively (D'Mello and Stoodley, 2015). Structural differences in the superior cerebellar peduncle (SCP), the major efferent white matter tract from the cerebellum to the cerebral cortex, and MCP show disruptions in pathways exiting the cerebellum. These structural abnormalities in the MCP and SCP highlight differences in the entire cerebro-cerebellar loop in ASD individuals: from the cerebral cortex to the cerebellar cortex and back again. This decreased integrity in cerebellar outflow pathways ultimately result in loss of modulatory input from the cerebellum to cortical regions involved in motor behavior and social processing. Evidence supporting the relationship between decreased FA in right and left SCPs and increased repetitive behaviors and social impairments in ASD, respectively, has been reported (Catani et al. 2008; Hanaie et al. 2013). The cerebellum is one of the most consistent sites related to pathophysiology in ASD, with differences reported from the cellular up to behavioral levels (Fatemi et al. 2012).

Cerebellar Neuropathology in ASD

Looking at the cellular level, many cerebellar structures are affected in ASD (Wang et al. 2018; Ellegood et al. 2015). Cerebellar hypoplasia and reduction in cerebellar cell counts are common neuropathologies observed in ASD individuals; more specifically, an ASD-related reduction in the number of Purkinje cells (PCs) from control subjects is one of the most frequently reported differences in post-mortem brains of autistic individuals (Table 1; DiCicco-Bloom et al. 2006). Post-mortem studies of ASD have measured a loss of PCs in cerebellar cortex (Fatemi et al, 2002; Bauman and Kemper, 2005), and found that the reduction in PCs is more pronounced in posterior inferior regions of the cerebellar hemispheres and less marked in the medial vermis (Bauman and Kemper, 1985).

Certain post-mortem studies of ASD brains have replicated this loss of PCs, most pronounced in the lateral hemispheres, while fewer studies have reported PC loss in the vermis (Bruchhage et al. 2018). PC loss appears to occur early in development, due to the absence of glial hyperplasia in the cerebellum of ASD patients (Bauman and Kemper, 2005). In addition, low packing density and a reduction in PC size have been reported in individuals with ASD (Whitney et al. 2009). Interestingly, PC density was found to be mostly affected in Crus I and II, an area heavily interconnected with the prefrontal cortex in both sexes (Skefos et al. 2014). In addition to reduced PC numbers, post-mortem studies have reported microanatomic cerebellar neuropathologies in ASD patients, such as excess of Bergmann glial cells, reduced size and number of deep cerebellar nuclei cells (fastigial, globose, and emboliform nuclei), and an active neuroinflammatory process within cerebellar white matter (Table 1; Bauman & Kemper, 1985; Rogers et al. 2013, Bruchhage et al. 2018). Data from human neuroimaging and animal studies converge on cerebellar right Crus I lobule, reporting differences in lobular volume, grey matter density, white matter integrity, functional activation patterns, and functional connectivity in right Crus I of individuals with ASD (Stoodley et al. 2017).

These cerebellar neuropathologies detected in ASD individuals are considered associated with the cognitive and motor impairments seen in the pathology (Rogers et al. 2013). Coming from other cerebellar pathologies, at a macroscopic level, cerebellar atrophy and acute cerebellar lesions result in many cognitive deficits such as impairments in attention, planning, verbal fluency, memory, and associative learning; where the degree of cerebellar volume reduction is correlated with the degree of cognitive impairments (Bracke-Tolkmitt et al. 1989; Botez-Marquard and Botez, 1993; Courchesne et al. 1994; Schmahmann and Sherman, 1998; Thoma et al. 2008; Baillieux et al. 2010). In addition to its inherent cognitive deficits, cerebellar changes in ASD also result in fine and gross motor deficits such as the lack of movement coordination, disturbances of accuracy of movements, impairments of gait and postures, and unstable balance (Rogers et al. 2013). These findings suggest that the cerebellar structural changes expressed in ASD could indeed be part of the substrate affecting the cognitive and behavioral phenotype.

Prenatal Valproic Acid (VPA) Exposure: A Rodent Model of ASD

To study in more detail the cerebellar-associated behavioral and structural differences in ASD, certain studies have focused on environmental influences to generate animal models of autism. Most cerebellar differences highlighted in human studies associated with social and communication impairments as well as repetitive behaviors of autistic patients are also seen in animal models of autism (D'Mello and Stoodley, 2015). Despite the strong genetic mutation etiology of ASD, approximately 90% of ASD cases are classified as idiopathic (Betancur, 2011). Interestingly, prenatal or perinatal environmental insults have been recently reported to play a role in the contribution to ASD (Rogers et al. 2013). In early development, the brain is susceptible to environmental insults from exposure to certain chemicals, such as ethyl alcohol, thalidomide, misoprostol, and VPA (Landrigan, 2010; Moore et al. 2000; Rodier, 2002; Bandim et al. 2003). Exposure to these chemicals causes neuropsychological changes similar to behavioral symptoms expressed in ASD individuals (Rogers et al. 2013).

Mechanisms of Action of VPA

Valproic acid (VPA) is an anticonvulsant and mood-stabilizing medication widely prescribed for the management of epilepsy and bipolar disorder (Favre et al. 2013). VPA's potential to act as a neuromodulator and a histone deacetylase inhibitor (HDAC) has been studied, allowing it to regulate gene expression through chromatin remodeling (Johannessen & Johannessen, 2003; Phiel et al. 2001). However, it is important to note that chronic administration of VPA during the first trimester of pregnancy has been associated with a range of abnormalities, including neural tube defects, structural cardiac abnormalities, polydactyly, neurodevelopmental delay, and craniosynostosis. Exposure to VPA *in utero* triples the risk of having a child with ASD (Moore et al. 2000). While the emergence of other neurodevelopmental disorders can occur after *in utero* VPA exposure, the development of ASD is most commonly observed (Bromley et al. 2013).

VPA may contribute to the development of ASD-like behaviors due to multiple mechanisms of action. First, VPA can act as an HDAC inhibitor: when rodents are exposed to VPA on gestational day (GD) 12.5, there is a transient hyperacetylation of H3 and H4, which are important histone proteins involved in the structure of chromatin in eukaryotic cells. Kataoka et al. (2013) show that the exposure also causes a transient increase in cellular apoptosis and a

decrease in cellular proliferation and migration in the embryonic brain (Kataoka et al. 2003). In addition, VPA has been found to inhibit glycogen-synthase kinase 3 (GSK-3β), which negatively regulates the Wnt-signaling pathway. This pathway is essential for axonal remodeling, cellular proliferation, embryonic patterning, and organogenesis (Chenn, 2008), and alterations in its activation can lead to abnormalities in cellular proliferation and migration of neuronal cells that are critical for the formation of neuronal networks in the developing embryo (Chen et al. 1999; Jung et al. 2008). Finally, VPA can disrupt the balance between excitatory and inhibitory activity in the developing brain. In rodents, injection of VPA on GD 12 results in the overexpression of glutamatergic transcriptional promoters and an increase in excitatory glutamatergic neuronal markers (Kim et al. 2014), while treatment with VPA leads to the downregulation of genes necessary for GABAergic inhibitory neuronal development (Fukuchi et al. 2009). Together, these findings indicate that the administration of VPA during the critical period of embryonic development may have a complex influence on the development of ASD-like behaviors.

Behavioral Cerebellar Pathologies in prenatally VPA-exposed Rodents

The administration of VPA has been used in rodents as an effective inducer to the expression of core autistic symptoms and changes brain circuitry. Indeed, VPA produces brain structure alterations, well-related to the ASD phenotype, in the offspring of rodent mothers exposed to the drug during pregnancy (Arndt et al. 2005). A list of cognitive and motor behavioral symptoms expressed in VPA-exposed rodents is given in Table 1; many of these are similar to the behaviors manifested in human patients with ASD. Some of the core behavioral symptoms expressed in ASD individuals include motor impairments such as repetitive/stereotyped behaviors, hyperactivity, poor social and communication skills, and deficits in cognitive functions such as attention (Table 1; Moore et al. 2000; Wang et al. 2014). Similarly, mice and rats prenatally exposed to VPA exhibit pathological behaviors including increased stereotypy, hyperactivity, decreased social play and exploratory behavior, decreased pre-pulse inhibition, and deficits in olfactory discrimination compared to the control rats (Table 1; Schneider and Przewlocki, 2005; Roullet et al. 2010).

AUTISM	HUMANS	RODENTS (VPA)
PATHOLOGICAL BEHAVIORS	Motor impairments such as repetitive/stereotyped behaviors [5]	Increased stereotypy [3,4]
	Hyperactivity [5]	Hyperactivity [2]
	Poor Social and Communication Skills [6]	Decreased Social Play and Exploratory Behavior [1]
	Deficits in Cognitive Functions (attention, planning, memory, verbal fluency, etc.) [6,7]	Decreased Prepulse Inhibition [1]
	Delayed Speech and Motor Development [8]	Deficits in Olfactory Discrimination [1]
CERBELLAR NEUROPATHOLOGIES	Decreased Purkinje cell number (more significant in posterior inferior regions of cerebellar hemispheres) [8,9]	Decreased Purkinje cell number (more significant in the posterior part of the cerebellum) [13,14,15]
	Cerebellar Hypoplasia [10]	Apoptosis of cerebellar cells [16]
	Neuroinflammation in Cerebellar White Matter [11,12]	Apoptosis of Granule Layer Cells [16]
	Reduced Size and Number of Fastigial, Globose, and Emboliform Nuclei Cells [11]	Injuries in Deep Cerebellar Nuclei (reduced interposed nuclei) [17]

Table 1: Summary of behavioral pathologies and cerebellar neuropathologies observed in VPA-exposed rodents (model of autism) and humans with ASD. [1] Schneider and Przewlocki, 2005 [2] Courchesne and Pierce, 2005; [3] Roullet et al. 2010; [4] Nicolini and Fahnestock, 2018; [5] Wang et al. 2014; [6] Sasson et al. 2013; [7] Schmahmann and Sherman, 1998; [8] Varghese et al. 2017; [9] DiCicco-Bloom et al. 2006; [10] Courchesne et al.1988; [11] Bauman & Kemper, 1985; [12] DeRamus and Kana, 2015; [13] Roux et al. 2019, [14] Yochum et al. 2008; [15] Ingram et al. 2000; [16] Wang et al. 2018; [17] Mowery et al. 2015.

The effect of VPA on the Neuroanatomy of the Cerebellum

Similar to individuals with ASD, VPA-exposed rats exhibit common structural cerebellar neuropathologies. In fact, Yochum et al. (2008) found that prenatal exposure to VPA in rats induced an increase in apoptotic cells in the cerebellum while Ingram et al. (2000) found that rodents prenatally exposed to VPA had approximately 30% fewer PCs compared to the control animals (Yochum et al. 2008; Ingram et al. 2000). These structural differences parallel the ones observed in ASD individuals. Additionally, due to higher prevalence of ASD in male compared to female subjects, Roux et al. (2019) investigated the differential susceptibility of PCs in VPA-exposed rodents and found a more pronounced PC loss in the posterior part of the cerebellum, including the VIth, VIIth, IXth lobules of the vermis, as well as the paramedian lobules of male compared to female VPA-exposed rats. These findings support a sex-specific susceptibility of PCs to VPA, which may contribute towards the sensorimotor disturbances and behavioral pathologies observed in ASD (Roux et al. 2019). In young rats exposed to VPA, in addition to the cerebellar PC loss, there appears to be an increased apoptosis in the external granule cell layer (Wang et al. 2018; Kim et al. 2013), and disruption of the nuclei morphology of the DCN (Wang et al. 2018; Mowery et al. 2015). Of course, besides the neurodevelopmental effects of VPA on the cerebellum, it also targets other regions, in the cerebral cortex and other structures. For instance, VPA induces a decrease in the number of hypoglossal motor neurons of the hypoglossal nuclei in prenatally VPA-exposed rats which plays a role in orofacial movements such as licking and/or drinking (Schneider and Przewlocki, 2005). Overall, the use of the VPA rodent model is commonly accepted to study the neurobiological mechanisms of ASD; however, the effect of VPA on cerebellar associated motor functions remains partially understood. The behavioral and neuroanatomical similarities support the use of the VPA-exposed rodents as a model for the study of ASD-like neuropathology, particularly as it relates to the study of circuit-level mechanisms, which we wish to apply to the cerebellum.

RATIONALE AND OBJECTIVES

As expressed above, cortico-cerebellar circuits play a role in the expression of sensorimotor and cognitive behaviors. The cerebellum mediates fine motor coordination and complex motor skill learning; additional recent evidence has revealed the role of the cerebellum in cognitive and psychiatric disorders including ASD. Patients diagnosed with ASD frequently present cerebellar associated motor and cognitive deficits such as stereotyped/repetitive movements and impairments in motor coordination as well as in social and communication behaviors since early childhood. The mechanisms through which cerebellar deficits may affect such functions in ASD are still under study.

With emerging research on ASD using whole-brain imaging, there is increasing evidence of neuroanatomical changes in various brain regions and alterations in neural connectivity. These studies have focused on gross macroscopic changes in the brain of ASD individuals, such as differences in the volumetric size of specific regions, cortical thickness, and white and grey-matter relations. In this vein, ASD was redefined from a disorder of ‘social relatedness’, to a disorder of altered connectivity, where the underdevelopment of critical neural pathways characterizes the emergence of abnormal information processing in ASD individuals (Just et al.

2004, 2007). Indeed, findings of decreased functional optimization in specific cerebro-cerebellar circuits have been associated with the core impairments in ASD (D'Mello and Stoodley, 2015) Based on recurring evidence, scientists have discovered that exposure to environmental factors during the prenatal stages, such as the valproic acid antiepileptic drug, contribute to the development of ASD. Although both rats and mice are similar in many aspects, rats present clear advantages in terms of larger brain size (making brain surgery manipulations easier) and lower stress during human contact (Ellenbroek & Youn, 2016). Prenatal exposure to VPA in rats triggers neuropathological processes presumably similar to the ones observed in human subjects with ASD. Cerebellar neuropathologies such as cerebellar atrophy, increased apoptosis of cerebellar PCs and DCN cells, and external granular cell layer (during development) are expressed in VPA-exposed rats.

The purpose of my project is to investigate the effect of prenatal VPA exposure on the cerebellar circuitry. At the level of cell numbers, we wish to evaluate the impact of the manipulation on the structure of the cerebellum and its various lobules and components. We will measure the counts in Purkinje and DCN cells, and the effect on GCL - using its thickness as a measure of cell numbers. We wish to apply a circuitry-level comparison, to see which component is most affected.

For this study, we will use three primary outcomes: (1) PC count and density, (2) GCL thickness measurements, and (3) DCN cell count and density; and one independent variable: treatment (saline vs. VPA). The correlation between PC density and GCL thickness will also be studied in both groups. To better report localization, PCs will be counted in the posterior and anterior lobes, as well as in the vermis and hemisphere lobules of the cerebellum. As for the DCN cells, they will be identified and counted according to the specific nucleus: medial and intermediate. The GCL thickness measurements will be measured across the lobules to better localize the changes due to the neurological model.

In this project, the cerebellar linear density of PCs and the GCL thickness, and their correlation will primarily be studied in two defined groups of male rats: VPA- and saline (SAL)-exposed rats. Secondarily, the DCN cell density in defined regions (medial and intermediate) will be quantified. In general, we hypothesize that PC and DCN cells will reflect differences in density, and the GCL will display differences in thickness between the VPA- and SAL-exposed male rats. We also believe that we will see the effects mainly localized to the cerebellar hemispheric lobules of the posterior lobe, and medial and intermediate nuclei of the DCN cells.

Specifically, we hypothesize we will find:

- A reduction in PC linear density, with a more significant loss in the cerebellar hemisphere lobules of the posterior lobe compared to the lobules of the anterior lobe and the vermis, in the VPA-exposed rats compared to control rats. The decreased cerebellar cell count density is supported by previous findings.
- A reduction in DCN cell counts and within-area density in the VPA-exposed rats compared to the control rats, as the DCN cells are directly linked to the PCs for output.
- A reduction in GCL thickness in VPA-treated rats compared to the control rats, more pronounced in the posterior lobules compared to the anterior lobules of the cerebellum.
- Correlation between the PC density and GCL thickness in control rats.

Materials and Methods

Animals and Housing

All experimental procedures followed the guidelines set by the Canadian Council on Animal Care and approved by the Animal Care Committee of Concordia University. Animals were housed and maintained by Dr. Sarah Ferraro from the Amir Laboratory at Concordia University. The animals used in this study were also used in circadian behavioral experiments (Ferraro et al. 2021). Briefly, time-pregnant naïve female Wistar rats (4 months of age) were purchased from Charles River Canada (Charles River, St-Constant, QC) and were delivered on gestational day (GD) 10. Dams were individually housed in clear plastic cages, under controlled conditions in the Concordia Animal Care Facility (temperature 20-21°C, 55%-65% humidity and 12h/12h light/dark cycle with lights on at 7:00 am and lights off at 7:00 pm). The rats were provided with *ad libitum* access to water and food. On GD 12, male dams received a single intraperitoneal injection of either VPA dissolved in saline (500 mg/kg, 1 ml/kg) or 0.9% saline solution (1 ml/kg) (Wang et al. 2018). This thus produced two groups of male pups: those whose mother had been given VPA (VPA group), or saline (saline group). On PND 23, the pups were weaned. Pups were introduced to sound-attenuated isolation boxes with *ad libitum* access to food and water (Ferraro et al. 2021).

Histological procedures

Tissue Preparation. At 14-18 weeks old, male rats from both groups were deeply anesthetized with sodium pentobarbital (100 mg/kg, intraperitoneally) and transcardially perfused with 300 ml of cold saline (0.9% NaCl), followed by 300 ml of cold paraformaldehyde (4% in a 0.1M phosphate buffer, pH 7.3). Brains, including the cerebellum, were extracted and post-fixed for 24 hours in paraformaldehyde at 4℃, then sliced coronally at 30 μm or 50 μm for staining and stored in -20℃ in Watson's Cryoprotectant. To discern rhythmic expression differences between groups, four time points for tissue harvesting were selected (Zeitgeber time (ZT) 1, 7, 13 and 19). This was done by Dr. Sarah Ferraro. For my project, we selected slices from ZT-7 and ZT-13 (because of a larger sample size collected during the mounting of the slices compared to the other ZT groups) for quantitative measurements of the cerebellar cells and networks.

Tissue staining. The cerebellar slices were stained with Cresyl Violet to reveal the cell bodies for cell counting. To wash off the cryoprotectant solution, the slices were first set in 10x PBS for 10 mins. The sections were later placed in another batch of 10x PBS to mount them onto gel-coated glass and left to air-dry thoroughly for 1-2 days. For the staining procedure, the brain sections were first rinsed with distilled water for 1 min for hydration, then transferred into a staining bath of Cresyl Violet dye (60℃) for 6 mins (depending on the intensity of the dye). To prepare the Cresyl Violet dye, 1g of powdered Cresyl Violet dye was added to 900 ml of distilled water, and the solution was heated to 60℃ to yield a 0.1% solution. To this mix, 4.5 ml of 10% glacial acetic acid solution was added while keeping the temperature at 60℃, and the solution was filtered to remove undissolved particles and prevent them from attaching to the brain slices. After dipping the sections into the dye, they were differentiated by rinsing with 95% ETOH for 30 s, then dehydrated using 99% ETOH for 5 mins, and finally cleared using Citrisolv (Fisher

Scientific, Pittsburgh, PA, USA) for 30 s. The slides were fixed with Permount, cover-slipped and left to dry for 24 to 48 hours.

Cellular Counts and Density Measurements

Tissue visualization and microscopy. Once the sections were mounted on gel-coated slides and stained with Cresyl Violet, they were examined using a regular light microscope, and selected slices were captured with a Nikon Livescan Sweptfield confocal microscope (Melville NY) housed in the Centre for Microscopy and Cellular Imaging (CMIC) at Concordia University (Figure 4). This CMIC microscope is equipped with lasers for confocal imaging, bright lenses, a motorized stage, and a Nikon Perfect Focus autofocus system. The bright lenses used for the capturing of the slices were set at 20x. The system included a digital camera (Photometrics CoolSNAP HQ2 CCD camera) with high-resolution imaging (13111 x 8589 pixels). The system is operated using the Nikon NIS-Elements software.

Localization of the lobules of the hemisphere and vermis. To localize the lobules in the coronal sections that were stained and captured, a rat brain atlas was used (Paxinos and Watson, 2013). The lobules of the cerebellar hemisphere which included the Simplex, Crus I, Crus II, Paramedian (PM) and the copula pyramidis (Cop) were located and labelled (See Figure 4-A, B). The lobules of the cerebellar vermis were more challenging to identify individually - mainly due to the coronal sectioning of the brain slices which did not permit to differentiate the individual lobules of the vermis as clearly as for the lobules of the hemisphere. Therefore, the lobules of the vermis were assembled into groups: lobule 1 was labeled as “Lobule 1”; lobules 3 and 4 were labelled as “Lobule 3-4”; lobule 5 was labelled as “Lobule 5” (Figure 4-C); lobules 6a, 6b, and 6c, were labelled as “Lobule 6”; lobules 7, 8, and 9 were labelled as “Lobule 7-8-9”; lobule 10 was labelled as “Lobule 10” (Figure 4-A,B).

Counting cells. We counted cells and measured GCL thickness using the ImageJ (http://imagej.nih.gov) software (Fiji version, ImageJ2, 2.3.0). The high-resolution images were opened in this software (at a scale where 0.86 μm = 1 pixel) and RBG colour adjustments were applied to the images to highlight the contrast of the stained cells. Image J permits to manually select cells, which we tracked for PCs, as well as automatically detect cells based on their contrast and shape, which we used for DCN cells.

Linear density of Purkinje cell. Due to the relatively large size and distinct shape of the PCs located in their own single layer of the cerebellar cortex, localization and quantification of PCs could be performed manually. As PCs are arranged linearly, they were individually counted using the Cell Counter setting in ImageJ. The length of the cerebellum PC layer of interest was also measured to compute linear density measurements. This provided a linear density of PCs; measured by the number of PC per mm (See example in Figure 5-A).

Within-Area density of deep cerebellar nuclei cell. The DCN cells are smaller in size compared to the PCs, but also differentiated from the rest of the cerebellar tissue as they contrast well with the surrounding white matter of the cerebellum. Because of this light/dark contrast, the DCN cells were automatically counted by selecting the regions of interest, adjusting the threshold, and analyzing the “particles” within a personalized size range option to target the cells of interest

(Fiji version, ImageJ2, 2.3.0). These were set using these options: (1) to set the threshold - Image > Adjust > Threshold, then (2) the particles were analyzed through the setting Analyze > Analyze particles and setting a size range between 100 and 1,000 pixels^2 and a circularity between 0 and 1. Each individual cell within these size and circularity ranges were selected, highlighted, and numbered in yellow (see example in Figure 5-B). The circular two-dimensional area for the selected region was measured to transform the counts in an area density for the DCN cells, providing values of number of DCN cell per mm^2 (Figure 5-B).

Granule cell layer (GCL) thickness. The GCL, which is very dense in small granule cell somas, and is adjacent to the PC layer, also stained strongly with the Cresyl Violet dye. Because of its high density (some of the highest in the whole brain), we measured the thickness of the layer has been measured as a proxy for the cell count. The thickness was measured perpendicular to the plane defined by its length and was collected using ImageJ by extending a drawn line across the layer (technically, drawing a line on the regions of interest throughout, and using the "Measure" option in μm; see the illustration in Figure 5-C). This thickness was measured at regular intervals along the lobules through the addition of a grid setup to 20,000 pixels^2.

(A)

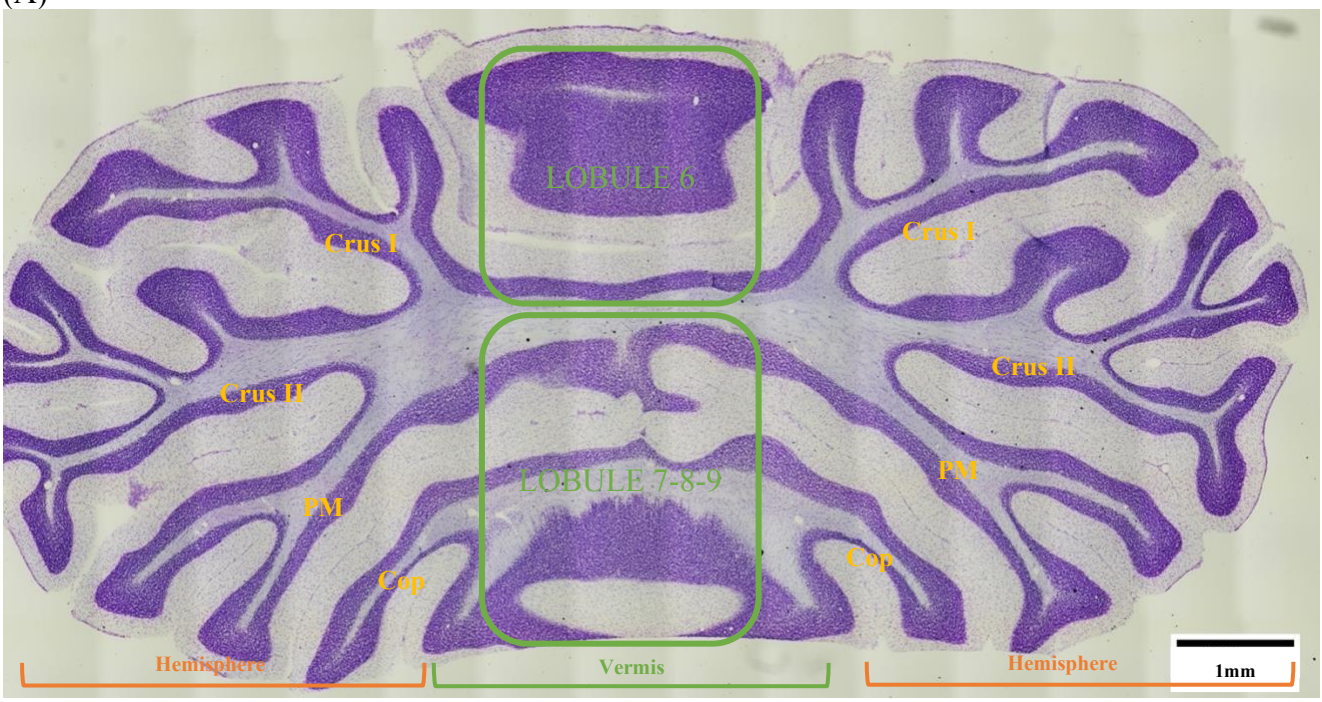
LOBULE 6
Crus I
Crus I
Crus II
Crus II
LOBULE 7-8-9
PM
PM
Cop
Cop
Hemisphere
Vermis
Hemisphere
1mm

(B)

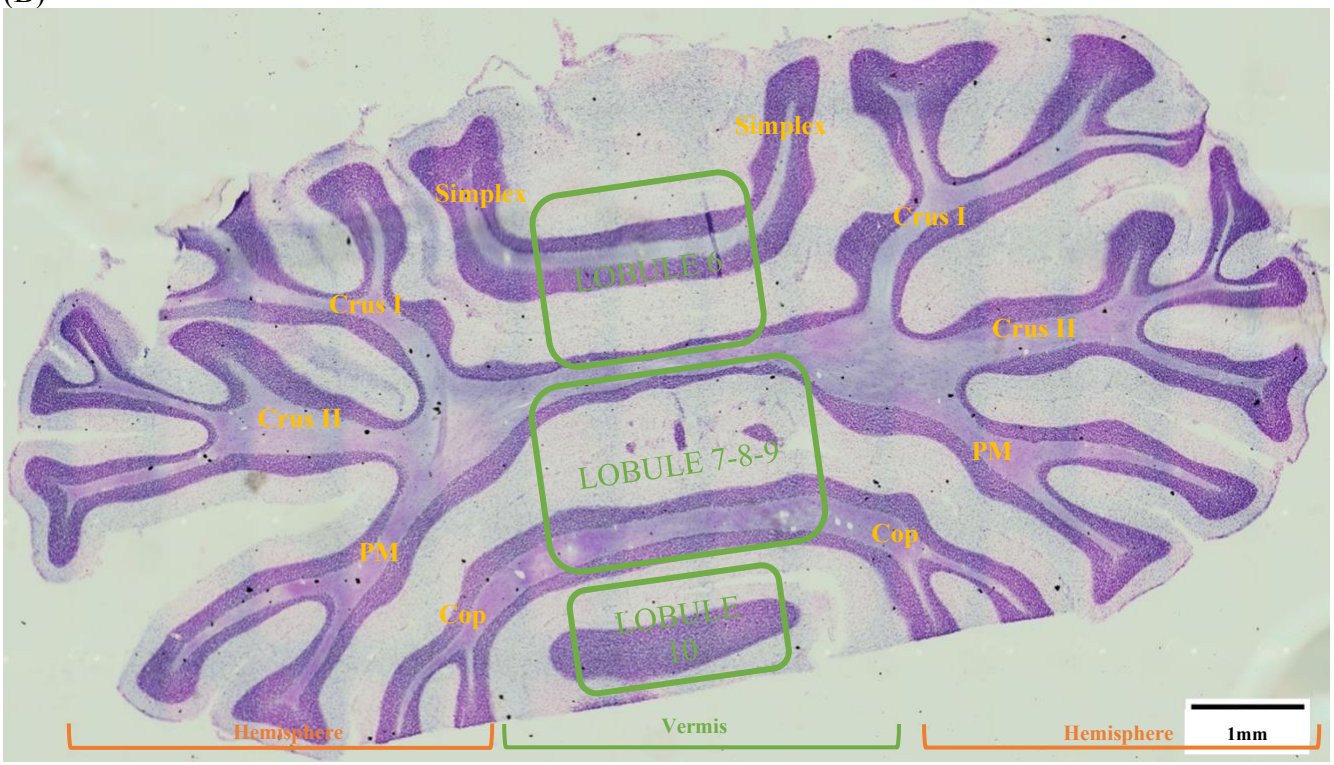
Simplex
Simplex
Crus I
LOBULE 6
Crus I
Crus II
Crus II
LOBULE 7-8-9
PM
PM
Cop
Cop
LOBULE 10
Hemisphere
Vermis
Hemisphere
1mm

(C)

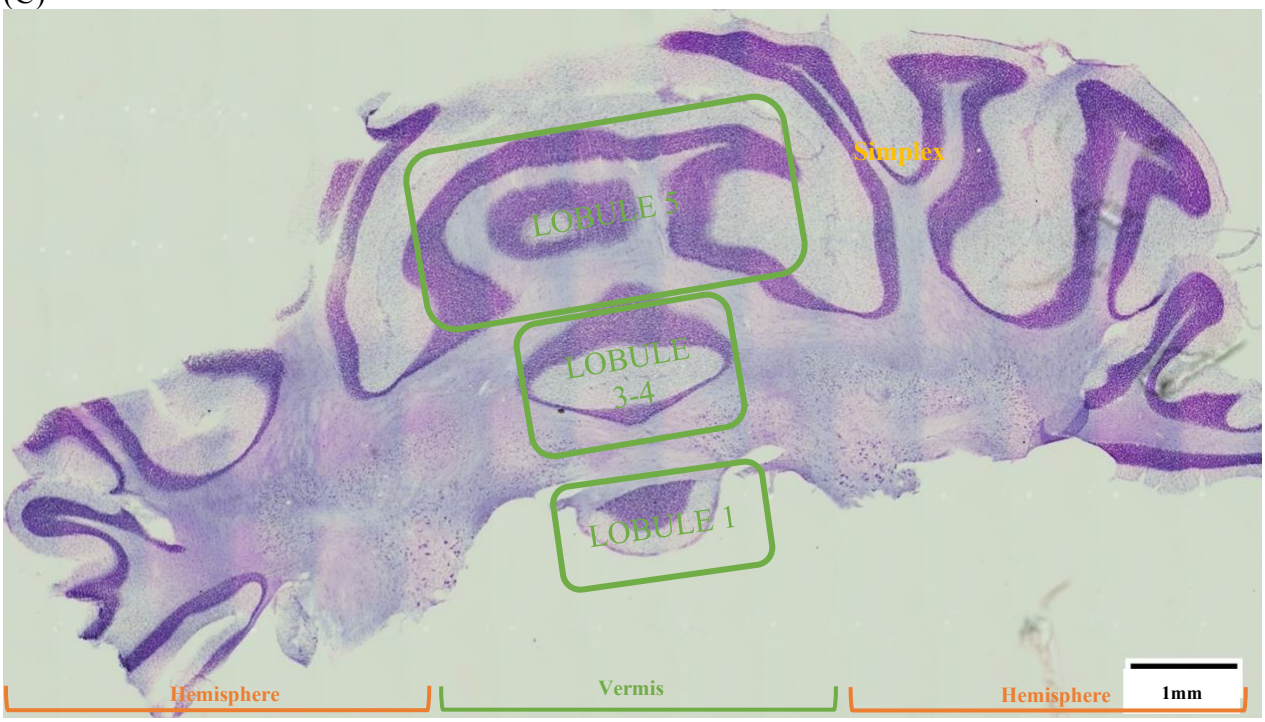
Simplex
LOBULE 5
LOBULE 3-4
LOBULE 1
Hemisphere
Vermis
Hemisphere
1mm

Figure 4: Captured and labeled coronal section from rat cerebellum. All sections are stained with Cresyl Violet from either VPA or Saline groups. The lobules of the cerebellar hemisphere which include the Simplex, Crus I, Crus II, Paramedian (PM) and copula pyramidis (Cop) are labelled in orange. The lobules of the cerebellar vermis which include Lobules 1, 3-4, 5, 6, 7-8-9, and 10 are labelled in green. All lobules were located using the cerebellar brain atlas (Paxinos and Watson, 2013).

(A)

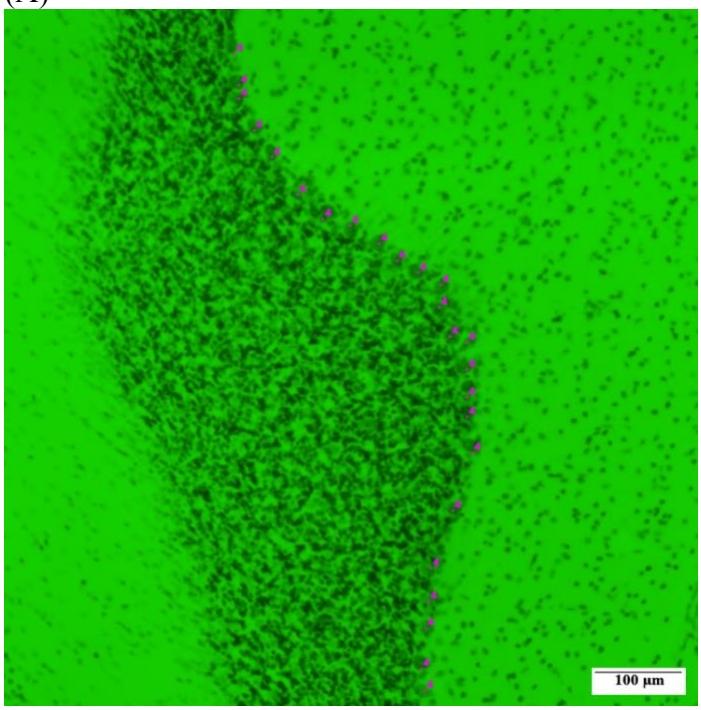

(B)

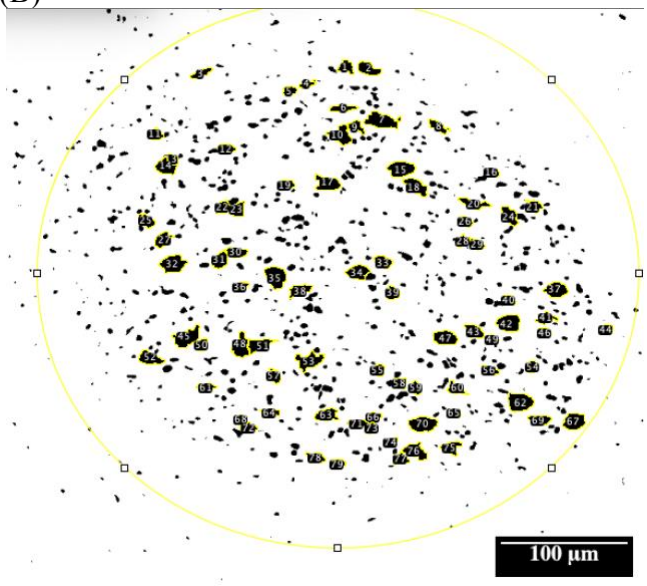

(C)

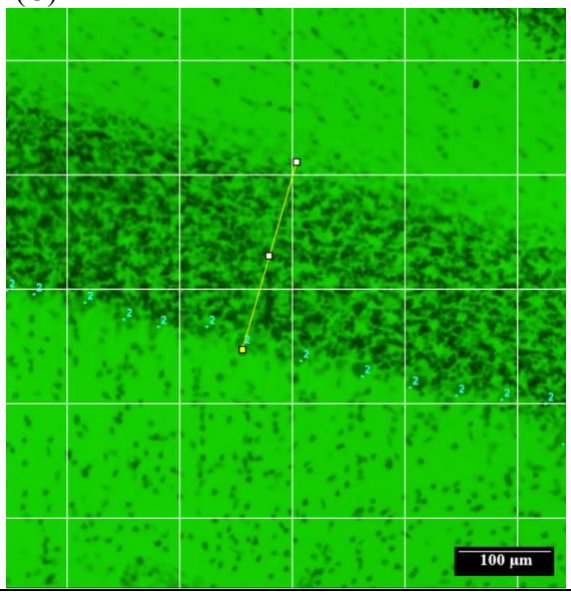

Figure 5: Measurement of cellular density in rat cerebellum. (A) PCs were identified as roundly shaped cells along the outer edge of the GCL. PCs were counted visually "by hand" using markers (in purple, as observed in this picture) across sections for the distance of the lobule. The linear density of PCs was expressed as the number of PCs/mm. (B) DCN cells were identified close to the white matter of the cerebellum and counted using adjusted detection algorithms in ImageJ. The yellow circle is the region of interest with the identified (numbered) DCN cells within. The area density of DCN cells is expressed as the number of DCN cells / mm^2. (C) GCL thickness measurement. The yellow line indicates the ImageJ linear measurement representing the GCL thickness. The layer thickness is measured in μm.

Co-localization of Purkinje cell density and GCL thickness

To connect functionally the circuit components of the cerebellum, an exploration of the relationship between the GCL thickness and the PC linear density was undertaken. To accomplish this, for one cerebellar slice (control animal R9, ZT1, slice 1_4), we related together the PC counts (n = 2018) with the GCL thickness measurements (n = 123). The PC and GCL two-dimensional location coordinates were used as localizations, superimposed on the high-resolution pictures coming from the microscopy process. This process was done using custom MATLAB code (MathWorks, Natick, MA, USA).

PC count processing. To complement the longer-scale linear density, we decided to try to calculate an instantaneous density for the PCs. Thus, we calculated X and Y difference in position between consecutive PCs (using the *diff* function), transformed the PC's X and Y differences into polar coordinates (using *cart2pol*), to gather a one-dimensional distance, and then divided 1000 μm by this value to establish a relative distance. After, we remapped all these values within a histogram distribution, color-coded to provide a heatmap along the lineup of the PC layer in the slice. A representation is shown in Figure 10-A.

GCL thickness processing. Here as well, we used the X and Y positions of the GCL thickness measurements. We remapped all these values relative to a histogram distribution, color-coded to a value of the thickness, plotted on the microscopy slice. Though we had fewer values, this helped to visualize the relative changes.

Relationship. With these PC and GCL values, we then established, for each GCL thickness value, the local average instantaneous density for the PCs. For each GCL thickness measure, a local PC linear density was established. Between two and eight values to assess a mean instantaneous density for the PCs, bordering and along an axis orthogonal to the GCL layer thickness. The result is a two-column matrix relating the 123 thicknesses with 123 PC densities. Because of some data uncertainty (in some cases near the thickness measurement, no PC were present due to tissue folds), we ended up with 114 valid dyads. The data were then fitted on a linear model, with a correlation value, and corresponding significance. These data are presented in Figure 11-A and B.

Cross-Covariance. To quantify a more instantaneous correlation between the GCL thickness and the linear density of PCs, we also evaluated the cross-covariance between the relevant data series. This evaluates the value-to-value similarity between two traces (similar to electrophysiology analysis - Frederick et al. 2022): we applied it here to see if the two layers were changing synchronously across the structure. The function used was *xcov* in MATLAB, normalized from -1 to +1. This provides a curve centered around zero-lag. The pattern of the curve informs on the relative alignment of the traces, and a coefficient of covariance can be extracted around the zero-lag.

Data analysis and statistics

All data are presented as mean +/- standard error of means (SEM). Each group of data has been tested for normality using the Kolmogorov-Smirnov test. Data that did not fit the Gaussian

distribution were compared using the non-parametric Kruskal-Wallis test. All statistical measures and graphs were performed using IBM SPSS Statistics software (https://www.ibm.com/spss, SPSS Statistics, v28.0.0.0). For PC count and linear density measurements across the lobules of the vermis and hemisphere regions, difference between groups were analyzed using a two-way analysis of variance (ANOVA). This test also examined whether the interaction between the group and lobule effects PC count and density. For DCN cell count and within-area density measurements between both groups, a two-way ANOVA was used. For the GCL thickness distribution, a non-parametric Kruskal-Wallis test was used. Finally, a linear regression test was performed to study the relationship between the GCL thickness and the PC density using MATLAB Statistical Toolbox. Planned comparisons were conducted with a Bonferroni correction when appropriate. Differences were considered significant when $p < 0.05$.

Results

To describe with clarity our dataset, here is a summary of the number of measurements taken for each of the variables that were studied (PC count, GCL thickness and DCN cell count). Overall, we had a sufficient number of slices to evaluate the posterior lobe of the cerebellum, but only had limited slices suitable for assessing the anterior lobe. This affected our capacity to count PCs and measure GCL thickness from the anterior lobe, as well as perform DCN cell counts.

(A)

Groups	Rat	Slice	PC count		
			Hemisphere	Vermis	TOTAL
CONTROL	Rat #1	Slice #1	1084	696	1780
		Slice #2	1764	659	2423
		Slice #3	1643	752	2395
		Slice #4	1672	677	2349
	Rat #2	Slice #1	1497	740	2237
		Slice #2	1529	829	2358
		Slice #3	1569	551	2120
	Rat #3	Slice #1	1360	1397	2757
		Slice #2	1471	496	1967
		Slice #3	1595	1136	2731
VPA	Rat #1	Slice #1	1031	858	1889
		Slice #2	1617	555	2172
		Slice #3	1202	457	1659
		Slice #4	1211	1024	2235
		Slice #5	1175	679	1854
	Rat #2	Slice #1	1197	412	1609
		Slice #2	498	622	1120
		Slice #3	1072	269	1341
		Slice #4	1324	659	1983
	Rat #3	Slice #1	901	956	1857
		Slice #2	1282	881	2163
		Slice #3	1099	881	1980
		Slice #4	1498	668	2166

(B)

Groups	Rat	Slice	GCL thickness measures		
			Hemisphere	Vermis	Total
CONTROL	Rat #1	Slice #1	126	91	217
		Slice #2	139	44	183
	Rat #2	Slice #1	114	43	157
		Slice #2	117	85	202
	Rat #3	Slice #1	146	47	193
		Slice #2	129	113	242
VPA	Rat #1	Slice #1	105	55	160
		Slice #2	101	55	156
		Slice #3	86	58	144
	Rat #2	Slice #1	112	39	151
		Slice #2	137	61	198
	Rat #3	Slice #1	128	77	205
		Slice #2	120	70	190

(C)

Groups	Rat	Slice	DCN cell count		
			Medial	Intermediate	Total
CONTROL	Rat #1	Slice #1	95	168	263
		Slice #2	98	149	247
		Slice #3	42	221	263
		Slice #4	22	149	171
	Rat #2	Slice #1	53	x	53
		Slice #2	24	x	24
		Slice #3	21	x	21
VPA	Rat #1	Slice #1	139	564	703
		Slice #2	140	170	310
		Slice #3	56	x	56
		Slice #4	73	x	73
		Slice #5	107	x	107
		Slice #6	101	x	101
		Slice #7	31	x	31
	Rat #2	Slice #1	79	x	79
		Slice #2	81	x	81
		Slice #3	124	328	452
		Slice #4	43	296	339
		Slice #5	119	324	443
		Slice #6	217	x	217
		Slice #7	83	158	241
		Slice #8	107	440	547
		Slice #9	58	x	58
		Slice #10	51	x	51
		Slice #11	43	x	43

Table 2: Dataset summary of the measurements collected in the project. (A) Dataset table of the number of PC count data collection in the lobules of the vermis and hemisphere, and the total of both lobules. (B) Dataset table of the GCL thickness measurements. (C) Dataset table of the DCN cell count data collection. Each table shows the number of rats and slices used for the data collection. The lobules of the cerebellar hemisphere include Simplex, Crus I, Crus II, paramedian and Copula pyramidis (Cop). The lobules of the cerebellar vermis include Lobule 6, Lobule 7-8-9 and Lobule 10.

Effects of valproate exposure on regional Purkinje cell counts

To investigate the anatomical effect of prenatal VPA-exposure on the development of the resulting offspring, the PC count and PC linear density were evaluated in control and VPA-exposed rats. The main results are shown in Figure 6, where the PC count and PC linear density are seen as varying across the lobules of the cerebellar hemisphere, and vermis. The represented lobules (where we had enough and consistent data to provide group assessments) of the cerebellar hemisphere include Simplex, Crus I, Crus II, Paramedian lobule (PM), and the Copula pyramidis (Cop) lobules, while the lobules of the cerebellar vermis include Lobule 6, 7-8-9, and 10.

PC cell count. From our ANOVA, we saw main effects between the lobules of the cerebellar hemisphere [$F(1, 100) = 29.446$, $p < 0.001$] and between the two groups (Control and VPA) [$F(1, 100) = 54.357$, $p < 0.001$] on PC count. In contrast, the interaction of the group and the lobules did not have a significant effect on the PC count [$F(1, 100) = 1.566$, $p = 0.189$]. The PC counts in most of the lobules of the cerebellar hemisphere were smaller in the VPA-exposed rats than the control group. In the VPA-exposed rats, there was a significantly smaller PC count only for lobules Crus II [$F(1, 100) = 1.489$, $p = 0.003$], Simplex [$F(1, 100) = 5.124$, $p = 0.26$], and the paramedian (PM) lobules [$F(1, 100) = 16.848$, $p < 0.001$] compared to the control counts (Figure 6-A; Table AP1-A in Appendix).

In contrast, from a separate ANOVA, we did not see a main lobule effect on the PC count between the lobules of the cerebellar vermis [$F(1, 46) = 2.695$, $p = 0.078$) nor did we see a main effect between the two groups [$F(1, 46) = 0.423$, $p = 0.519$). The interaction of the group and the lobules did not show a significant effect either [$F(1, 46) = 1.061$, $p = 0.354$) on the PC count. Interestingly, we observed a significant difference of PC count in the between-group pairwise comparison of Lobule 6 [$F(1, 46) = 5.326$, $p = 0.026$), which is the largest vermal lobules at the level of our sections. The PC count was significantly higher in the control group compared to the VPA-exposed rats. In contrast, we did not see significant differences in Lobule 7-8-9 [$F(1, 46) = 1.207$, $p = 0.278$] and Lobule 10 [$F(1, 46) = 0.323$, $p = 0.573$] between the two groups (Figure 6-C; Table AP1-C in Appendix).

PC linear density. There was a main group effect between the two groups [$F(1, 100) = 36.589$, $p < 0.001$] but no significant effect between the lobules of the cerebellar hemisphere [$F(1, 100) = 2.340$, $p = 0.06$] on the PC linear density. We can note that the influence of relative lobules length (in our slices) is here removed. Additionally, the interaction between the group and the lobules did not have a significant effect on PC linear density either [$F(1, 100) = 0.609$, $p = 0.657$]. In the pairwise comparisons, the PC linear density showed a significantly smaller values in the lobules Cop [$F(1, 100) = 13.713$, $p < 0.001$], Crus I [$F(1, 100) = 5.162$, $p = 0.025$], Crus II [$F(1, 100) = 9.446$, $p = 0.003$], and PM [$F(1, 100) = 10.007$, $p = 0.002$] of the cerebellar hemisphere in the VPA-treated rats compared to the control group (Figure 6-B; Table AP1-B in Appendix).

In contrast, the ANOVA on the lobules of the cerebellar vermis and the groups (VPA and Control) did not show a significant effect of group [$F(1, 46) = 0.168$, $p = 0.684$], or lobule [$F(1, 46) = 0.235$, $p = 0.792$] on the PC linear density. The group and lobules interaction did not show

any significant effects on PC linear density either [$F(1, 46) = 1.093$, $p = 0.344$). Even in pairwise comparisons, there were no significant differences in PC linear density observed for Lobule 6 [$F(1, 46) = 0.072$, $p = 0.79$], Lobule 7-8-9 [$F(1, 46) = 1.603$, $p = 0.212$], and Lobule 10 [$F(1, 46) = 0.722$, $p = 0.4$] of the cerebellar vermis between the two groups (Figure 6-D; Table 1-D in Appendix).

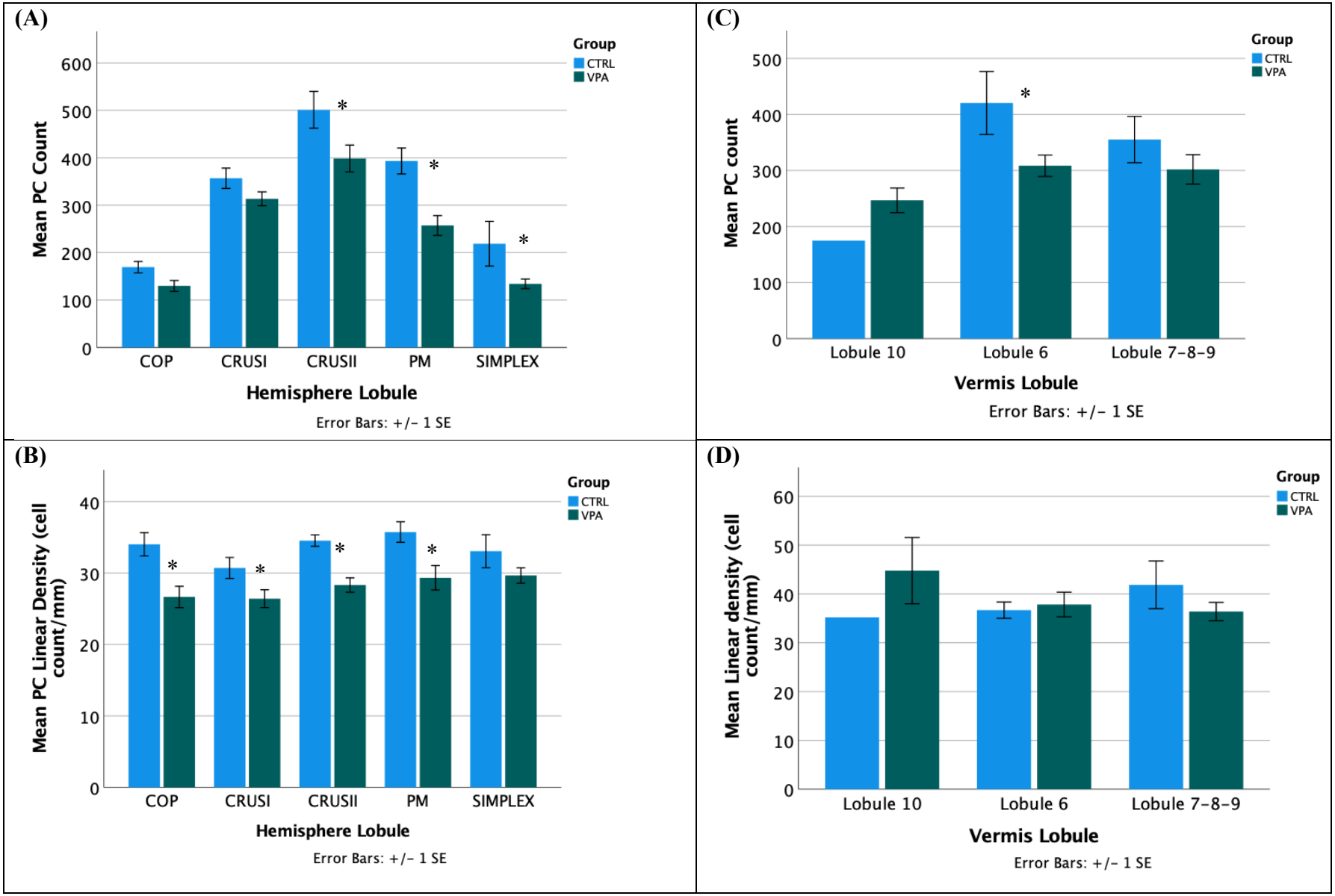
(A)
Mean PC Count
600
500
400
300
200
100
0
COP
CRUSI
CRUSII
PM
SIMPLEX
Hemisphere Lobule
Group
CTRL
VPA
Error Bars: +/- 1 SE
(C)
Mean PC count
500
400
300
200
100
0
Lobule 10
Lobule 6
Lobule 7-8-9
Vermis Lobule
Group
CTRL
VPA
Error Bars: +/- 1 SE
(B)
Mean PC Linear Density (cell count/mm)
40
30
20
10
0
COP
CRUSI
CRUSII
PM
SIMPLEX
Hemisphere Lobule
Group
CTRL
VPA
Error Bars: +/- 1 SE
(D)
Mean Linear density (cell count/mm)
60
50
40
30
20
10
0
Lobule 10
Lobule 6
Lobule 7-8-9
Vermis Lobule
Group
CTRL
VPA
Error Bars: +/- 1 SE

Figure 6: PC count and PC linear density for the two groups in lobules of the cerebellar hemisphere and vermis. (A, B) Average PC counts and PC linear density for different lobules of the cerebellar hemisphere in control and VPA-exposed rats. The lobules included in PC quantification of the cerebellar hemisphere are Simplex, Crus I, Crus II, Paramedian (PM), and Copula pyramidis (Cop). (C, D) Average PC counts and PC linear density for different lobules of the cerebellar vermis in control and VPA-exposed rats. The lobules included in PC quantification of the cerebellar hemisphere are Lobule 6, Lobule 7-8-9, and Lobule 10. The SE was not computed for Lobule 10. The blue and dark green bar represent the PC count in the control and VPA-exposed rat groups, respectively. The errors bars in black are also illustrated on each bar with a standard error (SE) of 1. Based on estimated marginal means, the star (*) is the significant mean difference at the 0.05 level. CTRL = Control group and VPA = VPA-exposed rats group.

Valproate effects on deep cerebellar nuclei cell counts and density in the two groups

Additionally, the DCN cell count and within-area DCN cell density were evaluated for each group and nucleus to further investigate the anatomical effect of prenatal VPA-exposure on the development of the cerebellar vermis. The DCN cell counts varied between the groups and showed significant differences in the intermediate and medial nucleus. Considering the small sample size collected for DCN data, we reported the sample size of slices throughout this section.

DCN cell count. From our ANOVA, we observed a main effect of nucleus on the DCN cell count between intermediate and medial DCN sectors (with the intermediate nucleus having more cells) [$F(1, 32) = 40.330$, $p<0.001$] and also a main effect of group with the VPA-exposed rats having a higher cell count than controls [$F(1, 32) = 12.174$, $p = 0.001$]. In contrast, the interaction of the group and nucleus did not show a significant effect on the DCN cell count [$F(1, 32) = 4.080$, $p = 0.052$] (Table 2-C). In pairwise comparisons, the VPA-exposed rats (with a sample size (n) = 4 slices) showed significantly higher counts in the intermediate nucleus compared to the control group (n = 7) [$F(1, 32) = 11.419$, $p = 0.002$]. The medial nucleus cell counts were not significantly affected between the two groups [$F(1, 32) = 1.608$, $p = 0.214$] (Figure 7-A; Table AP2-A, B in Appendix).

Within-area DCN cell density. We also computed the within-area density for DCN cells in both control and VPA-exposed rats and found that there were no main effects of nucleus between on between the intermediate and medial DCN sectors [$F(1, 32) = 1.685$, $p = 0.204$] nor a main effect of group [$F(1, 32) = 2.958$, $p = 0.095$]. The interaction of the group and nucleus did not show a significant effect either on the [$F(1, 32) = 0.546$, $p = 0.465$] (Table AP2-C in Appendix). Interestingly, we observed a significant difference in within-area DCN density in the pairwise comparison of the medial with a higher DCN density in the medial nucleus for the VPA-exposed rats (with a sample size of n = 18 slices) [$F(1, 32) = 4.503$, $p = 0.042$] compared to the control group (n = 7). The intermediate nucleus did not show this difference between the two groups [$F(1, 32) = 0.362$, $p = 0.551$] (Figure 7-B; Table AP2-A, C in Appendix).

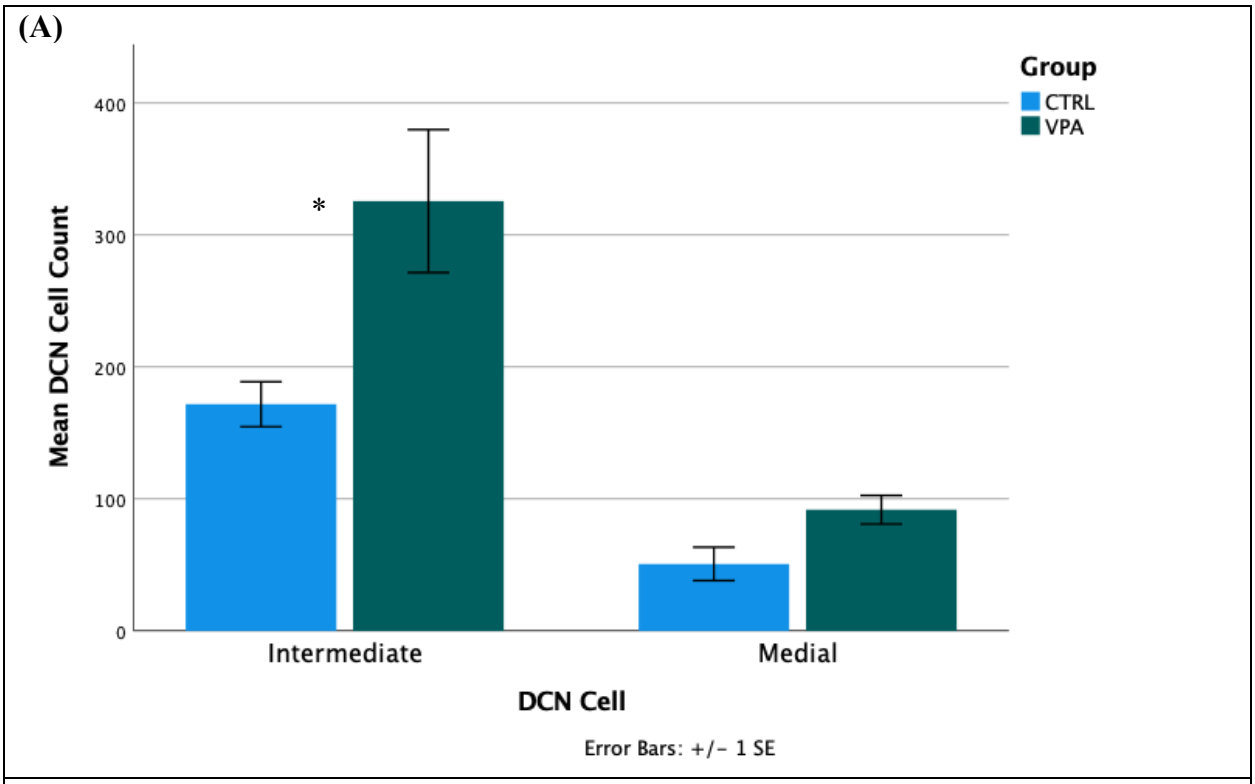
(A)
Group
CTRL
VPA
Mean DCN Cell Count
400
300
200
100
0
*
Intermediate
Medial
DCN Cell
Error Bars: +/- 1 SE

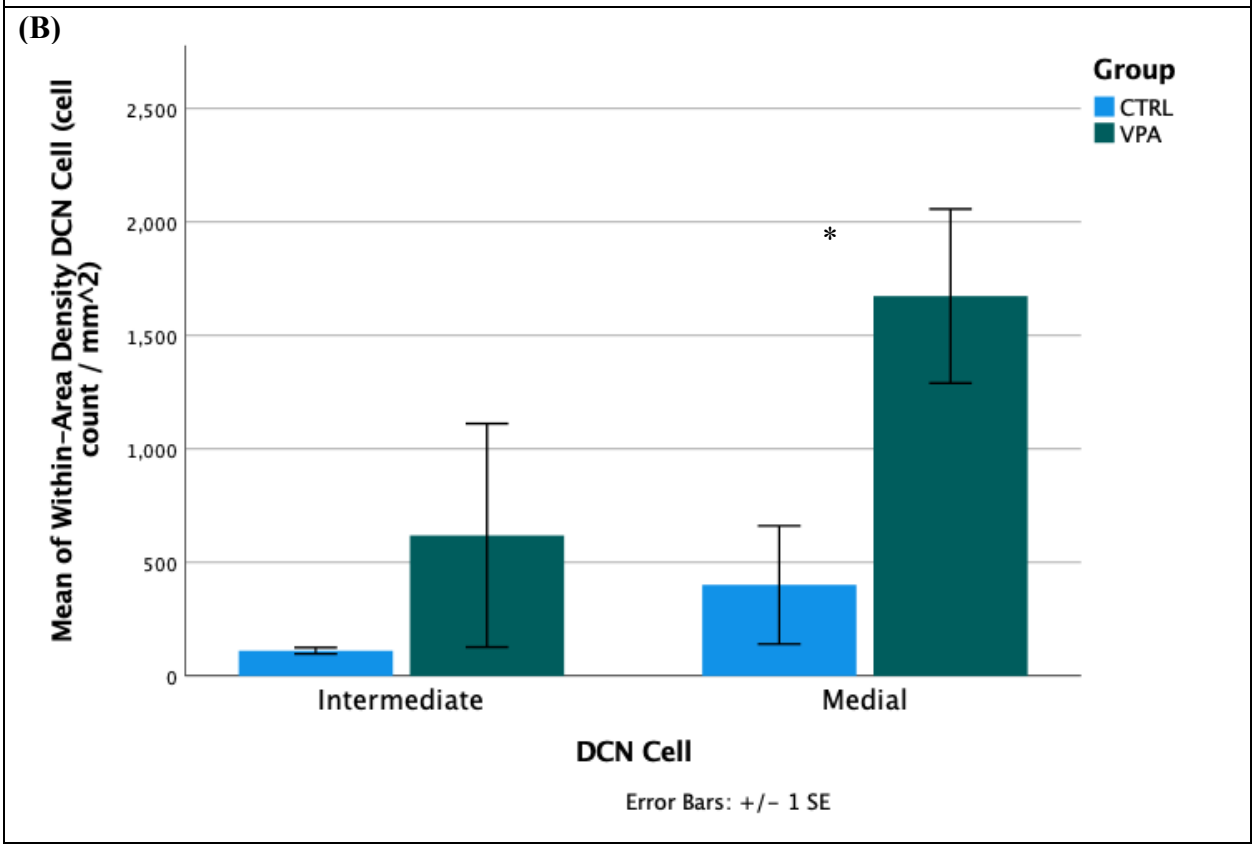
(B)
Group
CTRL
VPA
Mean of Within-Area Density DCN Cell (cell count / mm^2)
2,500
2,000
1,500
1,000
500
0
*
Intermediate
Medial
DCN Cell
Error Bars: +/- 1 SE

Figure 7: Prenatal VPA exposure effects on DCN cell count and within-area density of DCN cells in the intermediate and medial DCN sectors. Clustered bar graph of the mean of (A) DCN cell count and (B) within-area density of DCN cells in the intermediate and medial DCN sectors in control and VPA-exposed rats. The blue and dark green bar represent the PC count in the control and VPA-exposed rat groups, respectively. The errors bars in black are also illustrated on each bar with a standard error (SE) of 1. Based on estimated marginal means, the star (*) is the significant mean difference at the 0.05 level. CTRL = Control group and VPA = VPA-exposed rats group.

Effect of valproic acid on Granule cell layer (GCL) thickness distribution

To investigate the effect of VPA on the GCL thickness, we first measured the group effect across the combined lobules of the vermis and hemisphere from the cerebellum using our nonparametric statistical test (group comparison using the Kruskal-Wallis test). Following, we compared the individual lobules of the cerebellar hemispheres (Figure 8) as well as the individual lobules of the cerebellar vermis (Figure 9). We did not see a group effect for the GCL thickness distributions across the combined lobules of the cerebellar hemisphere and vermis between the two groups [Kruskal-Wallis H = 1.062, p = 0.302, df = 1] (Figure 8-F). In our lobule-specific analyses of the cerebellar hemisphere lobules, we did not see group effects either on the GCL thickness distribution across the Simplex [Kruskal-Wallis H = 0.009, p = 0.923, df = 1], Crus I [Kruskal-Wallis H = 0.340, p = 0.560, df = 1], Crus II [Kruskal-Wallis H = 0.392, p = 0.531, df = 1], PM [Kruskal-Wallis H = 0.157, p = 0.692, df = 1] and Cop [Kruskal-Wallis H = 6.854, p = 0.257, df = 1] (Figure 8).

Interestingly, the results were different for our vermal measurements. We did see group effects for the GCL thickness distribution in all the lobules of the cerebellar vermis. The VPA-exposed rats showed a significantly lower GCL thickness only in Lobule 6 [Kruskal-Wallis H = 27.454, p < 0.001, df = 1]), compared to the control group. In contrast, the VPA-exposed rats showed significantly higher GCL thickness in Lobule 7-8-9 [Kruskal-Wallis H = 6.854, p = 0.009, df = 1] and Lobule 10 [Kruskal-Wallis H = 23.106, p < 0.001, df = 1] compared to controls (Figure 9; Table AP3 in Appendix).

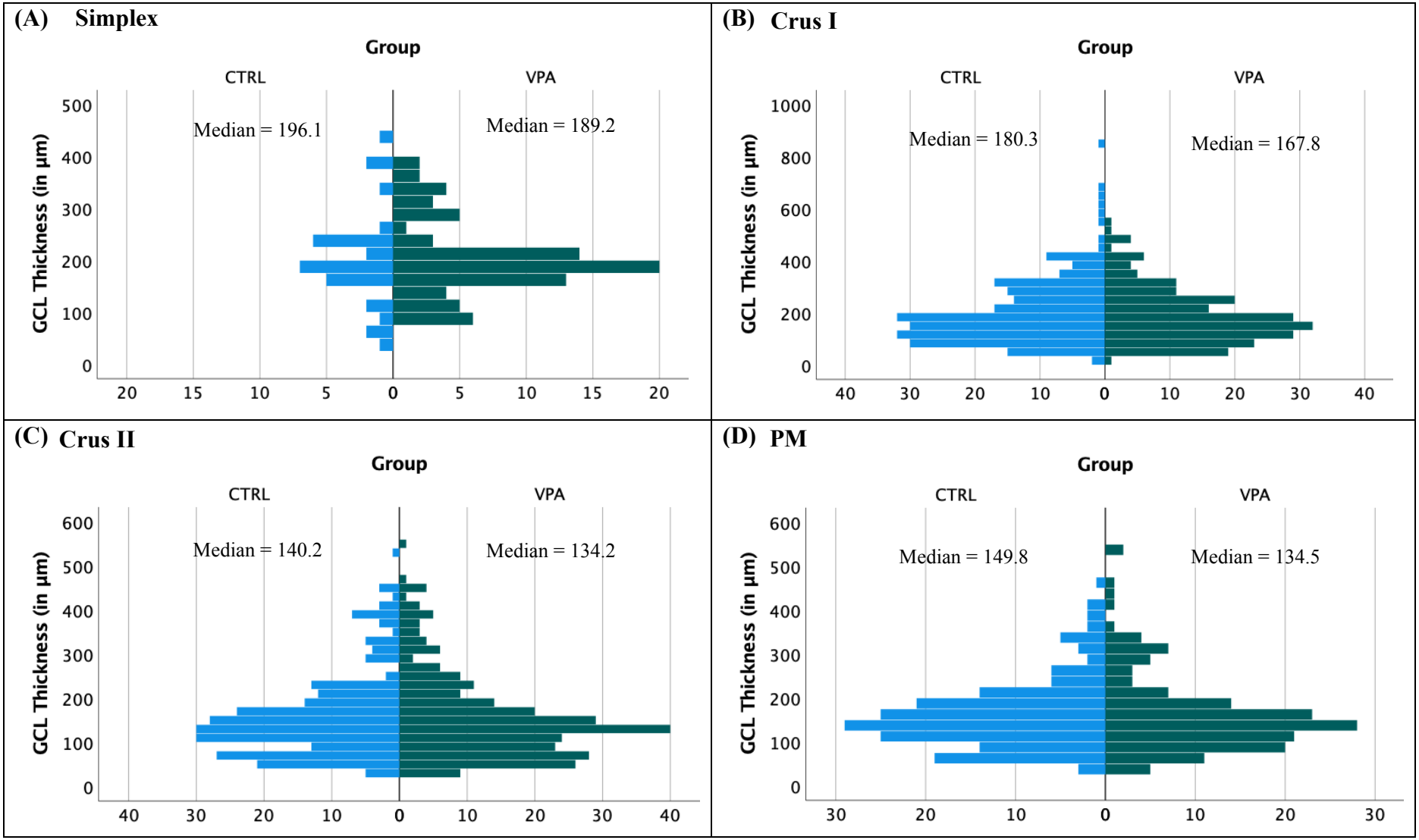
(A) Simplex
Group
CTRL
VPA
Median = 196.1
Median = 189.2
GCL Thickness (in µm)
(B) Crus I
Group
CTRL
VPA
Median = 180.3
Median = 167.8
GCL Thickness (in µm)
(C) Crus II
Group
CTRL
VPA
Median = 140.2
Median = 134.2
GCL Thickness (in µm)
(D) PM
Group
CTRL
VPA
Median = 149.8
Median = 134.5
GCL Thickness (in µm)

(E) Cop

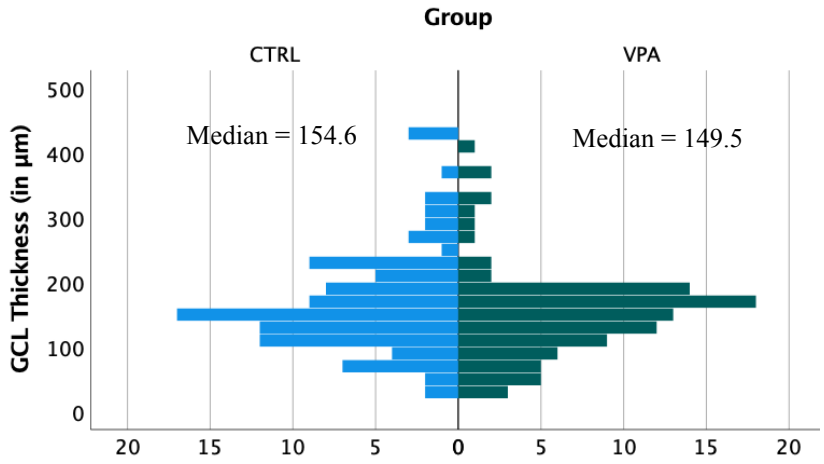

(F) Combined Lobules of the Vermis and Hemisphere

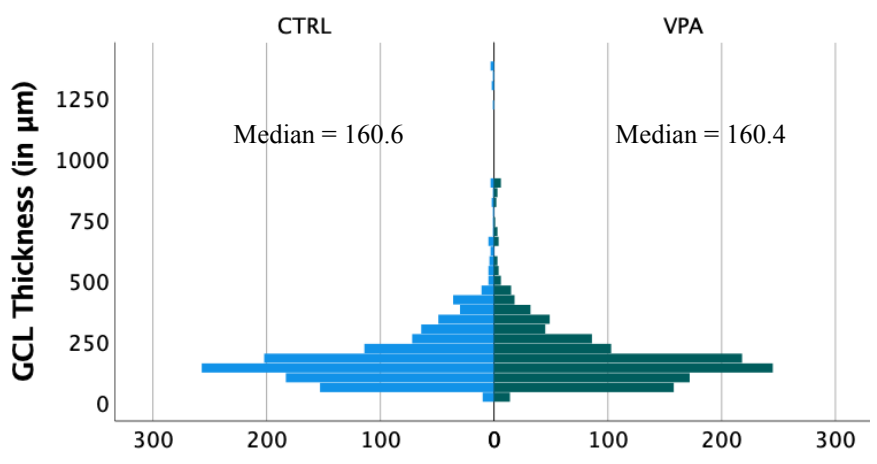

Figure 8: Pyramid frequency distribution of GCL thickness in the cerebellum and lobules of the cerebellar hemisphere. A, B, C, D, E represent the pyramid frequency distribution of GCL thickness of the Simplex, Crus I, Crus II, PM and Cop, respectively (in μm) in the Control and VPA-exposed rats. (F) Pyramid frequency distribution of GCL thickness across all the lobules of the vermis and hemisphere in the combined lobules of the vermis and hemisphere from the cerebellum in control vs VPA-exposed rats. The distribution on the left-hand side (in blue) represents the control group "CTRL", while the distribution on the right-hand side (in green) represents the experimental group "VPA". The mean rank of the GCL thickness measurements is reported for each of the groups in each lobule. CTRL = Control group and VPA = VPA-exposed rats group.

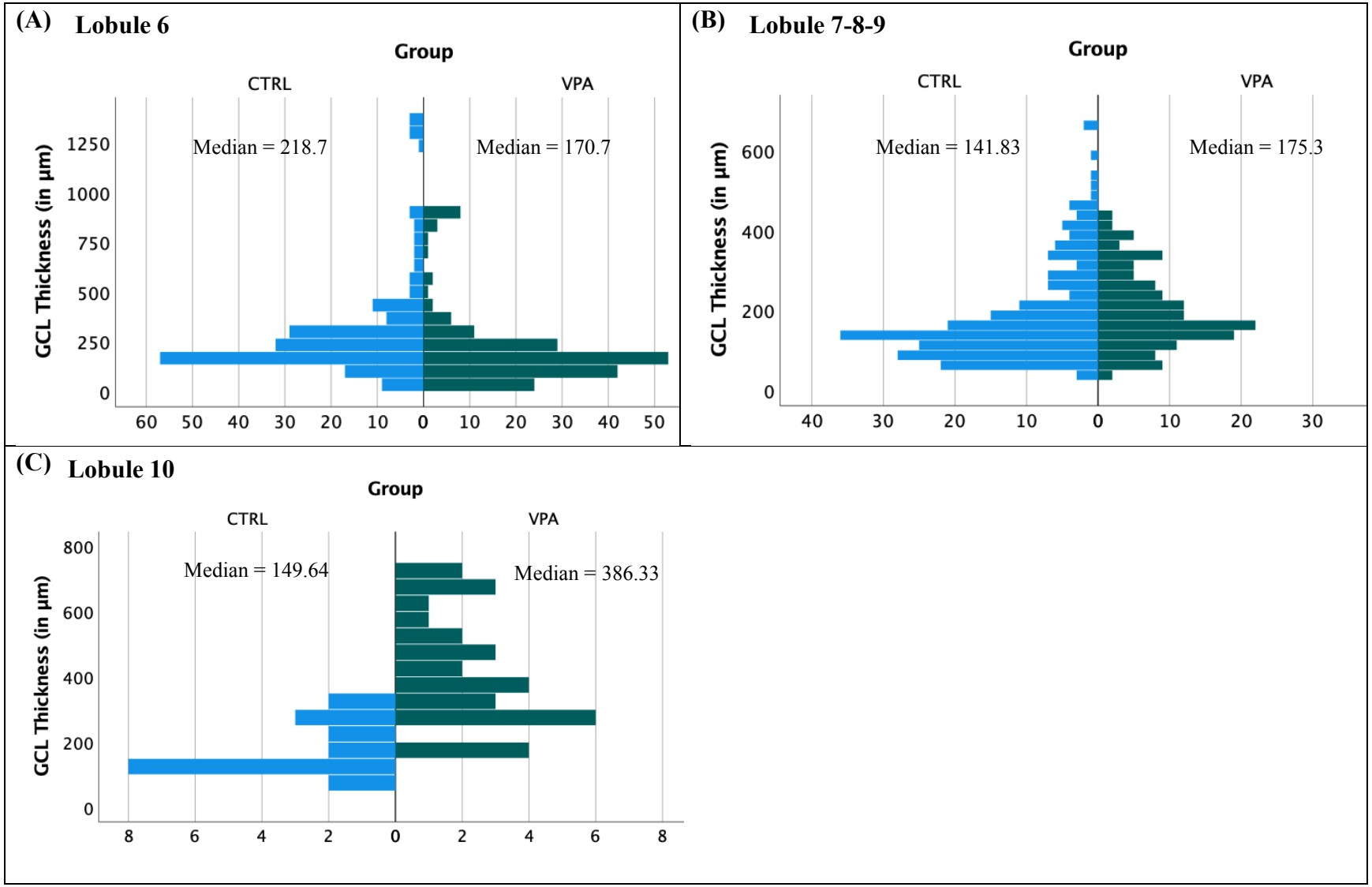
(A)
Lobule 6
Group
CTRL
VPA
GCL Thickness (in µm)
Median = 218.7
Median = 170.7
(B)
Lobule 7-8-9
Group
CTRL
VPA
GCL Thickness (in µm)
Median = 141.83
Median = 175.3
(C)
Lobule 10
Group
CTRL
VPA
GCL Thickness (in µm)
Median = 149.64
Median = 386.33

Figure 9: Pyramid frequency distribution of GCL thickness in the cerebellum and lobules of the cerebellar vermis. B, C, D represent a pyramid frequency distribution of GCL thickness of the Lobule 6, Lobule 7-8-9, and Lobule 10, respectively (in μm) in the Control vs. VPA-exposed rats. The distribution on the left-hand side (in blue) represents the control group "CTRL", while the distribution on the right-hand side (in green) represents the experimental group "VPA". The mean rank of the GCL thickness measurements is reported for each of the groups in each lobule. CTRL = Control group and VPA = VPA-exposed rats group.

Relationship between Purkinje cell and Granule Cell Layer thickness

To connect functionally the circuit components of the cerebellum (PC and GCL), an exploration of the relationship between the GCL thickness and the PC linear density was undertaken. To accomplish this, for one cerebellar slice (control animal R9, ZT1), we related together the PC counts (n=2018) with the GCL thickness measurements (n=123).

First used the X and Y coordinates of PC and GCL thickness values to provide a heatmap along the lineup of the PC and GCL layer (Figure 10). We observed an abundance of blue and green spots in the Simplex and Crus I lobules of the hemisphere which signified a relatively low density of PCs. In contrast, we noticed an abundance of yellow along the blue and green spots in the lobules of the posterior lobe (Crus II, PM and Cop) which signified a higher density of PC (Figure 10).

Correlation. Then, we performed the correlation of PC linear density and GCL thickness in all lobules of the cerebellar hemisphere (Figure 11-A) and the lobules of the posterior lobe (Figure 11-B). We found that there was no significant correlation between the variables in all the lobules of the cerebellar hemisphere ($p=0.15$; Figure 11-A). In contrast, we found that there a statistically significant correlation ($p<0.05$) between the PC linear density and the GCL thickness in the lobules of the posterior lobe (Figure 11-B).

Cross-Covariance. We analyzed the cross-covariance between the GCL thickness and the linear density of PCs for the sample data in the posterior lobe presented in Figure 12-A. The results are presented in Figure 12-B. In Figure 12-A, we see a consistent pattern of changes in GCL thickness and linear density of PCs across the lobules of the posterior lobe. This was confirmed by the cross-covariance shown in Figure 12-B, with a zero-lag synchrony, with a coefficient at 0.42. This hints at a dynamic relationship between GCL thickness and the linear density of PCs, sensitive to local circuit changes.

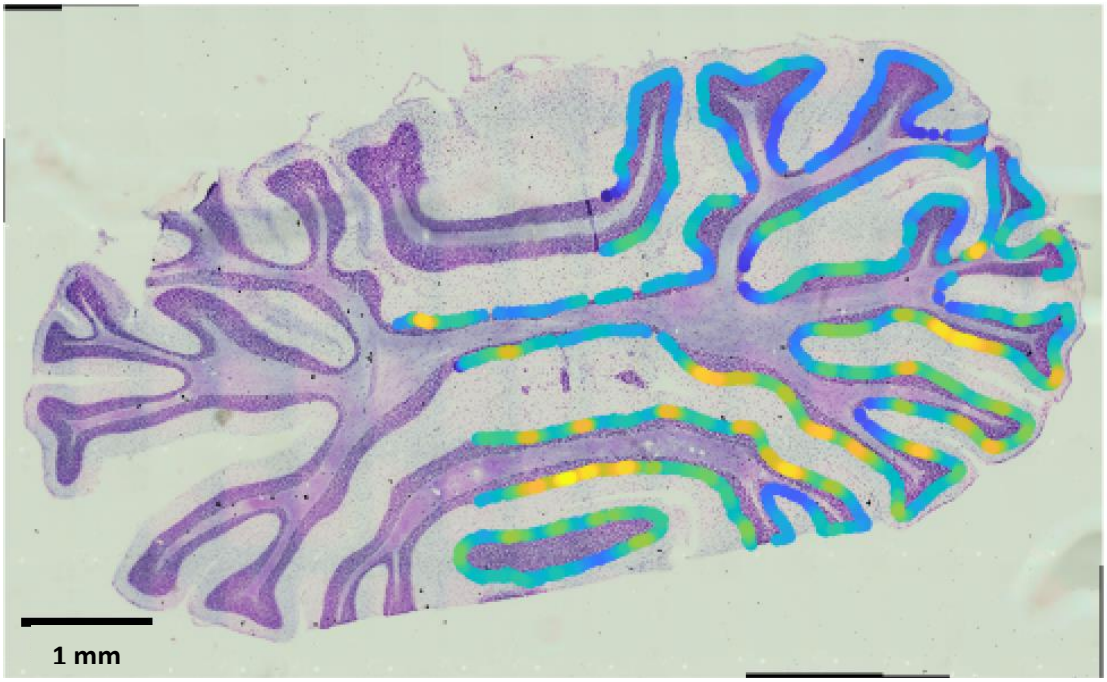

Figure 10: Heatmap representation of the PC linear density measurements. X and Y two-dimensional location coordinates of the PC are remapped relative to a histogram distribution. The colour grid on the right-end of both figures represents the intensity of the PC density (A). The yellow being the highest density measurement, and the dark blue being the lowest density measurement.

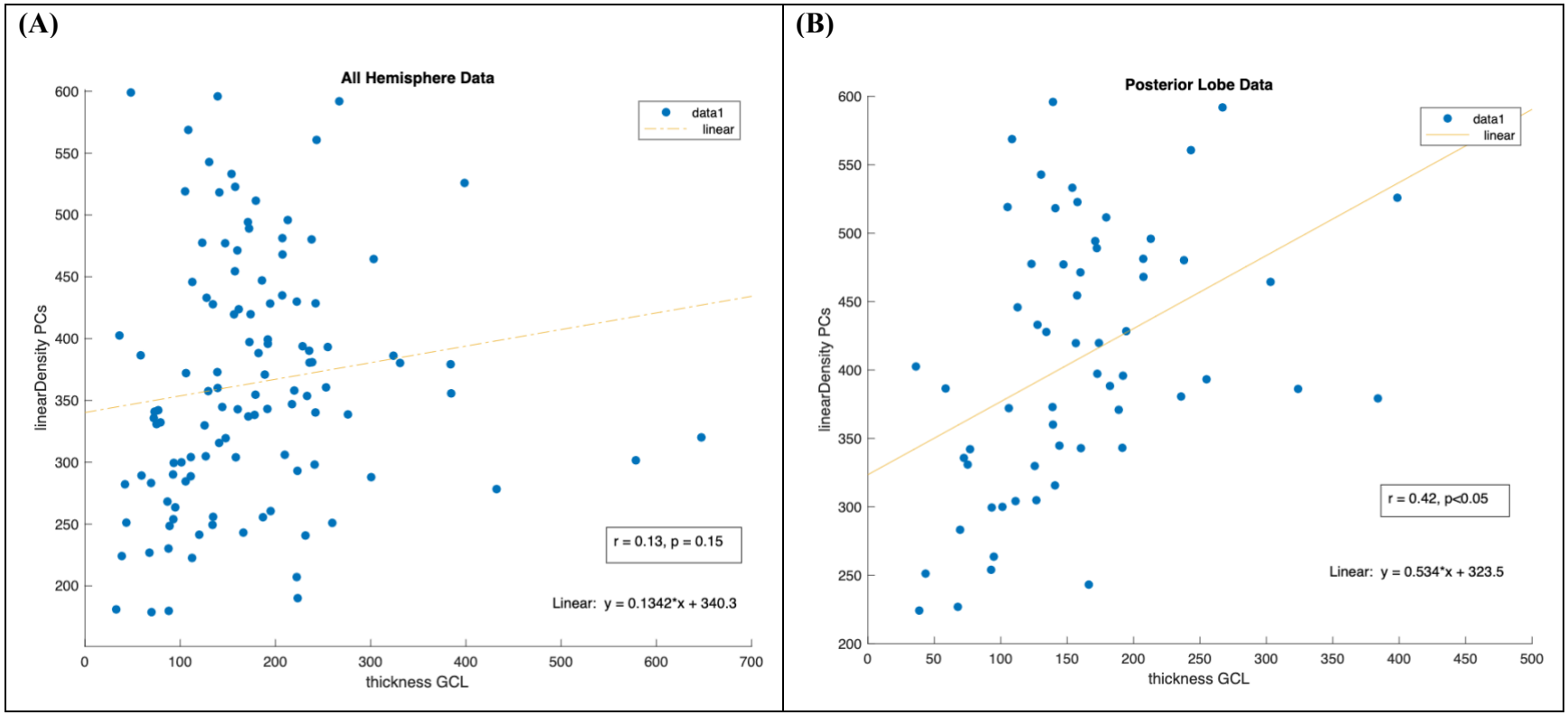
(A)
All Hemisphere Data
data1
linear
linearDensity PCs
thickness GCL
r = 0.13, p = 0.15
Linear: y = 0.1342*x + 340.3
(B)
Posterior Lobe Data
data1
linear
linearDensity PCs
thickness GCL
r = 0.42, p<0.05
Linear: y = 0.534*x + 323.5

Figure 11: Correlation between PC and GCL thickness in the posterior lobe and all hemisphere lobules. The x-axis represents the GCL thickness, and the y-axis represents the PC linear density. For each GCL thickness measure, a local PC linear density was established (with 123 data points) in (A) all lobules of the hemisphere region and (B) lobules of the posterior lobe. All the lobules of the hemisphere include Simplex, Crus I, Crus II, PM and Cop. The lobules of the posterior lobe include Crus II, PM and Cop. At the bottom right-end of the panel, the linear model with a correlation value (r) and corresponding significance is presented. The linear regression line is in yellow, and the data points are in blue.

(A)

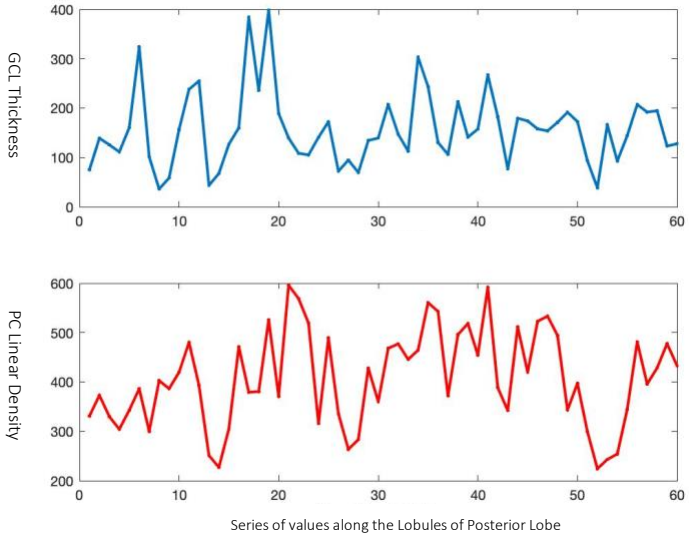
GCL Thickness
PC Linear Density
Series of values along the Lobules of Posterior Lobe

(B)

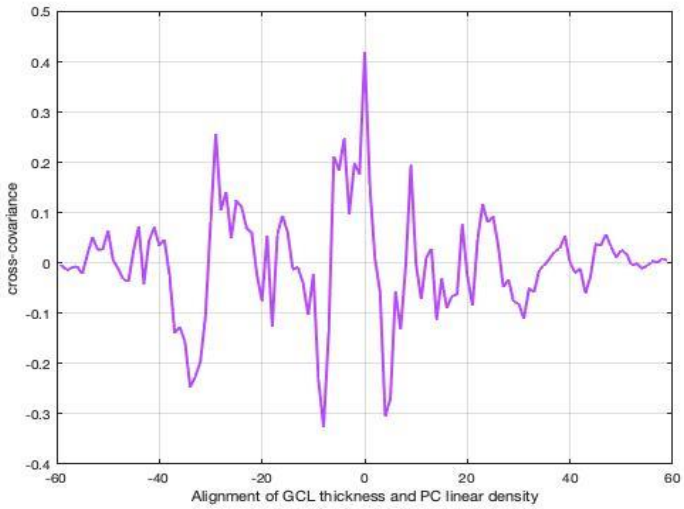
cross-covariance
Alignment of GCL thickness and PC linear density

Figure 12: Variation and cross-covariance of GCL thickness and PC linear density of the lobules in the posterior lobe. (A) Series of measurements of the GCL thickness (in the upper panel – in blue) and PC linear density (in the lower panel – in red). The x-axis represents the series of values of GCL thickness (in blue) and PC linear density (in red) along the lobules of the posterir lobe. The y-axis represents the GCL thickness (for the upper panel) and the PC linear density (for the lower panel). (B) The cross-covariance between the GCL thickness and the PC linear density. It is aligned on zero with a cross-covariance coefficient around 0.42. The y-axis represents the cross-covariance and the x-axis represents the alignment of GCL thickness and PC linear density. The lobules of the posterior lobe inlcude Crus II, PM and Cop.

Discussion

Here, we have provided several lines of evidence that demonstrate that VPA-exposed animal model of ASD shows cerebellar anatomy differences. First, we found that VPA-exposed rats displayed significantly lower PC count in the Simplex, Crus II and PM and lower PC density in lobules Crus I, Crus II, PM and Cop of the cerebellar hemisphere, compared to the control group. Second, considering the low number of cerebellar slices that contained DCN cells, we found that VPA-exposed rats displayed significantly higher counts in the intermediate nucleus, and higher density in the medial nucleus compared to the control group. Third, we found that VPA-exposed rats displayed significantly lower GCL thickness in Lobule 6, while higher GCL thickness was observed in Lobule 7-8-9 and Lobule 10 of the cerebellar vermis, compared to the control group. Finally, we found a significant correlation and cross-covariance between the PC and GCL thickness measurements in the lobules of the posterior lobe (Crus II, PM and Cop) in one control rat.

Effects of valproic acid on regional Purkinje cell count and linear density

In our study, we show that VPA-exposed rats have fewer PCs in the posterior part of the cerebellum, for specific lobules of the hemisphere. Previously, in ASD individuals, differences had been observed in the cerebellum, including cerebellar hypoplasia, reduced size and number of DCN cells, differences in lobular volume, grey matter density and white matter integrity in Crus I, and lower PC counts (Bruchhage et al. 2018; Wang et al. 2018; Ellegood et al. 2015; DiCicco-Bloom et al. 2006). Post-mortem studies of individuals with ASD have reported a loss of PCs in cerebellar cortex, more pronounced in the posterior inferior regions of the cerebellar hemisphere, when compared to the vermis (Bauman and Kemper, 2005; Bauman and Kemper, 1985). Interestingly, these areas functionally correspond with ASD signs: the posterior and inferior parts of the cerebellum are engaged in dynamic perceptual and affective processes with no explicit motor component (Nguyen et al. 2017). More specifically, motor and social deficits have been correlated with a loss of PCs in Crus I of VPA-exposed rats (Nguyen et al. 2017). This corresponds with our measurements of significantly smaller PC counts in lobules Simplex, Crus II, and PM of the hemisphere in the VPA-exposed rats. To normalize our PC counts relative to lobule length, we also parametrized our counts relative to measured lengths for each of the lobules, and thus calculated the PC linear density. The VPA-exposed rats still showed significantly smaller values in PC linear density in lobules Crus I, Crus II, PM and Cop of the hemisphere. On the other hand, in our measurements, the lobules of the cerebellar vermis did not show any significant differences between the two groups except for Lobule 6, contrary to what has been reported (Roux et al. 2019). We find part of the answer to this discrepancy in the fact that this differed from the PC linear density measurements. Nonetheless, our study showed a lower PC count and density in the VPA-exposed rats which were consistent with the literature (Ingram et al. 2000; Wang et al. 2018). More specifically, lobules 6 and PM were consistent with the significant loss of PC counts that has been reported in Roux et al. (2019) in the VPA-exposed rats (Roux et al. 2019). Although we had similar results reported as previous studies, our PC cell count is higher than other studies in the posterior lobe, providing us with better specificity for these lobules of the hemisphere.

Effects of valproic acid on deep cerebellar nuclei cell count and within-area density

The DCN cells are directly linked to the PCs and represent the general link of the cerebellar cortex to the rest of the brain and spinal cord. Anatomically, from the perspective of a coronally-sliced inspection of the cerebellum, the DCN are mostly present in the anterior lobe of the cerebellum, which proved to be a challenge for our quantification – the available samples did not provide many slices with nuclei. Several post-mortem studies have reported on the morphology of nuclei, including the size and number of cells in fastigial, globose, and emboliform deep cerebellar nuclei in individuals with ASD (Bauman & Kemper, 1985; Rogers et al. 2013; Bruchhage et al. 2018). Similarly, studies on VPA-exposed rats have reported disrupted morphology of these nuclei, including the nuclei length, area, and cell number of DCN, although further investigation is needed to understand the extent of these changes (Wang et al. 2018; Mowery et al. 2015). In our own study, we observed significant differences in the DCN cell count in only the intermediate nucleus cells in the VPA-exposed rats. This is unlike our PC quantification, where our VPA group had lower cell counts: here our DCN cell counts for VPA-exposed rats were higher compared to the control. Although the results were not statistically significant, this higher DCN cell count was also observed in the medial nucleus.

Part of this effect could have been explained by the location where the nucleus had been sliced: imagining the nucleus as an oblong egg, slicing at different levels would provide for large differences in surface area, strongly influencing the cell counts. We were concerned by the low number of slices with clear nuclei, and in the nuclei size variations. A mitigation measure was to normalize the DCN measurements, and we measured the area within the selected regions of the DCN cell count and calculated the "within-area density" of the DCN cells. Still, the VPA-exposed rats showed significantly higher values in the within-area density of DCN for the medial nucleus.

The other level of explanation could then certainly be our sample size for slices with nuclei cells, which was fairly small. As such, the cerebellar slices used for this study only had a small number coming from the anterior lobe (which is where most of the DCN cells are located). Therefore, the data for DCN cells were relatively small and inconsistent in both groups (Table 2-B). More data, and more slices with strong nucleus representation, would be needed for a conclusive assessment. Nonetheless, our present study did motivate to further explore the effect of VPA on DCN cell count and density, which has been understudied in the literature.

The effect of valproic acid on granule cell layer thickness

In a relatively new method of analysis, we also aimed at completing the analysis of the cerebellar circuits by complementing PC count with its afferent circuit components, the granule cells, located in its own layer (the GCL). In the VPA-treated animals during development, the GCL is affected: the external granule cell layer of the cerebellar cortex showed differences as well (during neural development, there are transitionally two layers: an internal GCL, and an external GCL). Specifically, Wang et al. (2018) and Kim et al. (2013) reported increased apoptosis of the external granule cell layer in VPA-exposed rodents (Wang et al. 2018; Kim et al. 2013).

Alternatively, granule cells were reported with smaller mean nuclear diameter in VPA-exposed rats compared to control, in addition to the PCs decrease (Alpay & Yucel, 2022).

In our own study, we measured the GCL thickness across the lobules of the hemisphere and vermis to further study the differences in the VPA-exposed rats. While measuring the GCL thickness distribution, we likely had a length-of lobule bias – the longer the lobule, the more thickness measurements were taken. We tried to be systematic in our measurements: as mentioned in the Materials and Methods section, we measured GCL thickness every 2 squares of a set grid to stay consistent. In our hands, no group effect was present throughout – certainly not across the cerebellar hemisphere. However, we did see a group effect on the GCL thickness of the lobules of the cerebellar vermis which were lower in Lobule 6, but higher in Lobule 7-8-9 and Lobule 10 in VPA-exposed rats compared to the control group. We are thus reporting a new result, showing that VPA had different effects on the GCL thickness across the lobules of the cerebellar vermis in the posterior lobe – this had not been reported previously.

Nevertheless, as a limitation, it is important to note that the coronally-sliced cerebellar slices used in this study might not have been the most appropriate plane to investigate and locate cell variables in the lobules of the cerebellar vermis. A better localization of the lobules of the vermis would be more obviously highlighted in sagittal slices of the cerebellum. It would be a good additional study to confirm our GCL thickness results, in the hemisphere and vermis, along the sagittal plane.

Correlation of Purkinje cell and Granule Cell Layer thickness

To further investigate the cerebellar connectivity, we wanted to study the relationship between the PC linear density and GCL thickness across the lobules of the cerebellar hemisphere. In terms of circuit functionality, PC and GCL layers interact strongly.

Using this new method of analysis, admittedly in a very small sample (1 slice with hard-fought quantification), we found that there is a significant correlation between the PC density and GCL thickness in the lobules of the posterior lobe. This should be interpreted carefully, as when the whole hemisphere was considered, no significant correlation was found. Of course, these data were only collected from one slice of a control rat - this is not enough to draw conclusions, but it is an impetus to systematize and structure an algorithm. This potential link between the PC density and GCL thickness calls for further investigation in VPA-exposed rats. Such functional links will likely be crucial for understanding the interactions between the circuit components of the cerebellum.

To quantify a more instantaneous correlation between the GCL thickness and the PC linear density, we performed the cross-covariance between the relevant data series. Interestingly, we also found a strong cross-covariance coefficient in support of the significant correlation previously reported. We also showed the variation of the PC linear density and GCL thickness values across the posterior lobe and noticed that the two quantities are interrelated “moment-to-moment”. In other words, the variation of both variables seems to be connected throughout the lobules of the posterior lobe. However, these results are only performed on one slice from a

control rat; therefore, more data is needed to show a statistical significance for the correlation and cross-covariance between GCL thickness and PC linear density.

These analyses should also extend to lobules of the vermis. From our results, VPA exposure affected the PC density in cerebellar hemisphere lobules but not their GCL thickness. In contrast, VPA exposure gave smaller PC counts in Lobule 6 of the vermis while affecting its GCL thickness. This could lead to a lobule-specific variation in the ratios between these cell layers, as affected by VPA exposure; this is certainly interesting as a further investigation.

Limitations of data collection and the VPA model

Getting access to VPA-treated rodent anatomical cerebellar slices proved to be a very valuable opportunity and data-rich set of samples, opening to many windows of analysis. This said, although this project produced interesting results, there were a number of limitations in this thesis work. The first two being more technical, and the last one being more theoretical.

First, our samples were coronally sliced, good for some quantification, but suboptimal for others. The coronal slicing of the cerebellar sections was challenging for the identification and localization of the lobules of the cerebellar vermis. For this reason, we had to group some of the lobules of the vermis to avoid misidentification of the individual lobules. This might have caused lack of specificity and data collection compared to the lobules of the cerebellar hemisphere which were relatively clear to identify. For future studies, it would be more appropriate to section the cerebellar slices sagittally, rather than coronally, where all the cerebellar lobules would be clearly located.

Second, we encountered a low number of cerebellar slices that contained the DCN (i.e., limited in slices from the anterior lobe of the cerebellum). This is likely caused by the sampling, which was limited to some cerebellar slices, located more posteriorly. A more remote but potential possibility for low DCN cells counts could be section manipulation. Some sections might have degraded in quality while stored in the cryoprotectant solution at -80 °C, or the tissues were lost or torn during the mounting process. As a result of the lack of DCN cell count data, we likely obtained inconsistent data and saw large differences in sample size between the two groups and two nuclei. The misidentification of intermediate or medial DCN cells may have affected the accuracy of the cell count data. To mitigate this issue, a more effective approach for analyzing specific DCN cells would be to select a region of interest and measure the area difference across all cerebellar slices containing DCN cells. This technique would provide a better understanding of whether the cell counting is consistent across DCN locations.

Third, in a more theoretical criticism, although the VPA-model of ASD is advantageous and replicates the behavioural and molecular differences associated with idiopathic ASD, most individuals with ASD have not been exposed to this drug *in utero*, suggesting that findings from this model may be limited. This is inherent to the model: individuals with ASD likely have not been exposed to certain environmental neural development inhibitors during gestational days. Nonetheless, the etiology of ASD is likely multifactorial in nature, converging onto similar molecular and cellular pathways leading to the development of the disorder and its effects on the

cerebellar circuitry. We show here that the use of a VPA model offers a controlled opportunity for the study of mesoscopic cerebellar circuitry disturbances in ASD.

Conclusion and future studies

To conclude, prenatal exposure to VPA was found to affect PCs density, specifically in lobules Crus I, Crus II, PM and Cop of the hemisphere in the posterior region of the cerebellum, and to affect GCL thickness in the Lobule 6, Lobule 7-8-9, and Lobule 10 of the vermis. For the DCN cells, although some of the results were statistically significant in the intermediate and medial nuclei, more data is needed to support the data obtained. Finally, the relationship (correlation and cross-covariance) between the PC and GCL thickness needs to be further investigated in the control group with more data, but also by comparing the relationship in the control with the one in VPA-exposed rats.

All these findings further raise the question to investing the cerebellar circuitry involved in ASD pathophysiology or ASD-like behaviors and the relevance of the specific cerebellar lobules in ASD behaviors. This body of research also emphasizes the urgent need for novel perspectives of ASD-associated comorbidities and highlights the nature of cerebellar circuitry in the disorder. For a while, it has been discovered that ASD is more prevalent in males compared to female individuals, therefore it would also be interesting to study the sexual dimorphism of VPA exposure on the cerebellar circuit.

References

Alpay, M., & Yucel, F. (2022). Changes of cerebellar cortex in a valproic acid-induced rat model of autism. *International Journal of Developmental Neuroscience*, *82*(7), 606–614. https://doi.org/10.1002/jdn.10213

American Psychiatric Association, A. (2013). *Diagnostic and statistical manual of mental disorders* (5th ed.). https://doi.org/https://doi.org/10.1176/appi.books.9780890425596

Arndt, T., Guessregen, B., Hohl, A., & Reis, J. (2005). Determination of serum amantadine by liquid chromatography-tandem mass spectrometry. *Clinica Chimica Acta; International Journal of Clinical Chemistry*, *359*(1–2), 125–131. https://doi.org/10.1016/j.cccn.2005.03.040

Baillieux, H., De Smet, H. J., Dobbeleir, A., Paquier, P. F., De Deyn, P. P., & Mariën, P. (2010). Cognitive and affective disturbances following focal cerebellar damage in adults: A neuropsychological and SPECT study. *Cortex; a Journal Devoted to the Study of the Nervous System and Behavior*, *46*(7), 869–879. https://doi.org/10.1016/j.cortex.2009.09.002

Bandim, J. M., Ventura, L. O., Miller, M. T., Almeida, H. C., & Costa, A. E. S. (2003). Autism and Möbius sequence: An exploratory study of children in northeastern Brazil. *Arquivos De Neuro-Psiquiatria*, *61*(2A), 181–185. https://doi.org/10.1590/s0004-282x2003000200004

Bauman, M., & Kemper, T. L. (1985). Histoanatomic observations of the brain in early infantile autism. *Neurology*, *35*(6), 866–874. https://doi.org/10.1212/wnl.35.6.866

Bauman, M. L., and Kemper, T. L. (2005). Neuroanatomic observations of the brain in autism: a review and future directions. *Int. J. Dev. Neurosci.* 23, 183–187. doi: 10.1016/j.ijdevneu.2004.09.006

Betancur, C. (2011). Etiological heterogeneity in autism spectrum disorders: More than 100 genetic and genomic disorders and still counting. *Brain Research*, *1380*, 42–77. https://doi.org/10.1016/j.brainres.2010.11.078

Botez-Marquard, T., and Botez, M. I., (1993). Cognitive behavior in heredodegenerative ataxias. *Eur.Neurol.* 33, 351-357. https://doi.org/10.1159/000116970.

Bracke-Tolkmitt, R., Linden, A., Canavan, A. G. M., Rockstroh, B., Scholz, E., Wessel, K., & Diener, H.-C. (1989). The cerebellum contributes to mental skills. *Behavioral Neuroscience*, *103*(2), 442–446. https://doi.org/10.1037/0735-7044.103.2.442

Brissenden, J. A., Tobyne, S. M., Osher, D. E., Levin, E. J., Halko, M. A., & Somers, D. C. (2018). Topographic Cortico-cerebellar Networks Revealed by Visual Attention and Working Memory. *Current Biology*, *28*(21), 3364-3372.e5. https://doi.org/10.1016/j.cub.2018.08.059

Bromley, R. L., Mawer, G. E., Briggs, M., Cheyne, C., Clayton-smith, J., García-fiñana, M., Kneen, R., Lucas, S. B., Shallcross, R., Baker, G. A., & Behalf, O. (2013). *The prevalence of neurodevelopmental disorders in children prenatally exposed to antiepileptic drugs*. 637–643. https://doi.org/10.1136/jnnp-2012-304270

Bruchhage, M. M. K., Bucci, M.-P., & Becker, E. B. E. (2018). Chapter 4—Cerebellar involvement in autism and ADHD. In M. Manto & T. A. G. M. Huisman (Eds.), *Handbook of Clinical Neurology* (Vol. 155, pp. 61–72). Elsevier. https://doi.org/10.1016/B978-0-444-64189-2.00004-4

Catani, M., Jones, D. K., Daly, E., Embiricos, N., Deeley, Q., Pugliese, L., et al. (2008). Altered

cerebellar feedback projections in Asperger syndrome. *Neuroimage* 41, 1184–1191. doi: 10.1016/j.neuroimage.2008.03.041

Chenn, A. (2008). Wnt/β-catenin signaling in cerebral cortical development Anjen. *Organogenesis*, *6278*, 76–80. https://doi.org/10.4161/org.4.2.5852

Chen, G., Huang, L., Jiang, Y., & Manji, H. K. (1999). *The Mood-Stabilizing Agent Valproate Inhibits the Activity of Glycogen Synthase Kinase-3*. 1327–1330.

Clark KA, Nuechterlein KH, Asarnow RF, Hamilton LS, Phillips OR, Hageman NS, Woods RP, Alger JR, Toga AW, Narr KL (2011). Mean diffusivity and fractional anisotropy as indicators of disease and genetic liability to schizophrenia. J Psychiatr Res. 2011 Jul;45(7):980-8. doi: 10.1016/j.jpsychires.2011.01.006. Epub 2011 Feb 8. PMID: 21306734; PMCID: PMC3109158.

Courchesne, E., Townsend, J., Akshoomoff, N. A., Saitoh, O., Yeung-Courchesne, R., Lincoln, A. J., James, H. E., Haas, R. H., Schreibman, L., & Lau, L. (1994). Impairment in shifting attention in autistic and cerebellar patients. *Behavioral Neuroscience*, *108*(5), 848–865. https://doi.org/10.1037//0735-7044.108.5.848

Courchesne, Eric, & Pierce, K. (2005). Brain overgrowth in autism during a critical time in development: Implications for frontal pyramidal neuron and interneuron development and connectivity. *International Journal of Developmental Neuroscience: The Official Journal of the International Society for Developmental Neuroscience*, *23*(2–3), 153–170. https://doi.org/10.1016/j.ijdevneu.2005.01.003

Courchesne, E., Yeung-Courchesne, R., Press, G. A., Hesselink, J. R., & Jernigan, T. L. (1988). Hypoplasia of cerebellar vermal lobules VI and VII in autism. *The New England Journal of Medicine*, *318*(21), 1349–1354. https://doi.org/10.1056/NEJM198805263182102

DiCicco-Bloom, E., Lord, C., Zwaigenbaum, L., Courchesne, E., Dager, S. R., Schmitz, C., Schultz, R. T., Crawley, J., & Young, L. J. (2006). The developmental neurobiology of autism spectrum disorder. *The Journal of neuroscience: the official journal of the Society for Neuroscience*, *26*(26), 6897–6906. https://doi.org/10.1523/JNEUROSCI.1712-06.2006

D'Mello, A. M., & Stoodley, C. J. (2015). Cerebro-cerebellar circuits in autism spectrum disorder. *Frontiers in Neuroscience*, *9*. https://www.frontiersin.org/article/10.3389/fnins.2015.00408

DeRamus, T. P., & Kana, R. K. (2015). Anatomical likelihood estimation meta-analysis of grey and white matter anomalies in autism spectrum disorders. *NeuroImage. Clinical*, *7*, 525–536. https://doi.org/10.1016/j.nicl.2014.11.004

Ellegood, J., Anagnostou, E., Babineau, B. A., Crawley, J. N., Lin, L., Genestine, M., DiCicco-Bloom, E., Lai, J. K. Y., Foster, J. A., Peñagarikano, O., Geschwind, D. H., Pacey, L. K., Hampson, D. R., Laliberté, C. L., Mills, A. A., Tam, E., Osborne, L. R., Kouser, M., Espinosa-Becerra, F., … Lerch, J. P. (2015). Clustering autism: Using neuroanatomical differences in 26 mouse models to gain insight into the heterogeneity. *Molecular Psychiatry*, *20*(1), 118–125. https://doi.org/10.1038/mp.2014.98

Ellenbroek, B., & Youn, J. (2016). Rodent models in neuroscience research: Is it a rat race? *Disease Models & Mechanisms*, *9*(10), 1079–1087. https://doi.org/10.1242/dmm.026120

Fatemi, S. H., Aldinger, K. A., Ashwood, P., Bauman, M. L., Blaha, C. D., Blatt, G. J., Chauhan, A., Chauhan, V., Dager, S. R., Dickson, P. E., Estes, A. M., Goldowitz, D., Heck, D. H., Kemper, T. L., King, B. H., Martin, L. A., Millen, K. J., Mittleman, G., Mosconi, M. W.,

… Welsh, J. P. (2012). Consensus paper: Pathological role of the cerebellum in autism. *Cerebellum*, *11*(3), 777–807. https://doi.org/10.1007/s12311-012-0355-9

Fatemi, S. H., Halt, A. R., Realmuto, G., Earle, J., Kist, D. A., Thuras, P., et al. (2002). Purkinje cell size is reduced in cerebellum of patients with Autism. *Cell. Mol. Neurobiol.* 22, 171–175. doi: 10.1023/A:1019861721160

Favre, M. R., Barkat, T. R., LaMendola, D., Khazen, G., Markram, H., & Markram, K. (2013). General developmental health in the VPA-rat model of autism. *Frontiers in Behavioral Neuroscience*, *7*(JUL), 1–11. https://doi.org/10.3389/fnbeh.2013.00088

Ferraro et al. (2021): *In utero* Exposure to Valproic-Acid Alters Circadian Organisation and Clock-Gene Expression: Implications for Autism Spectrum Disorders. Frontiers in Behav Neurosci, Vol 15, Article 711549, pp. 1-17.2

Frederick, A., Bourget-Murray, J., Tremblay, S.T., and Courtemanche, R. (2022): Local Field Potential, Synchrony of. In: Encyclopedia of Computational Neuroscience (edited by D. Jaeger, R. Jung and A. Destexhe). Springer 2nd Ed. DOI https://doi.org/10.1007/978-1-4614-7320-6_731-2

Fukuchi, M., Nii, T., Ishimaru, N., Minamino, A., Hara, D., & Takasaki, I. (2009). Valproic acid induces up- or down-regulation of gene expression responsible for the neuronal excitation and inhibition in rat cortical neurons through its epigenetic actions. *Neuroscience Research*, *65*, 35–43. https://doi.org/10.1016/j.neures.2009.05.002

Gill, J. S., & Sillitoe, R. V. (2019). Functional Outcomes of Cerebellar Malformations. *Frontiers in Cellular Neuroscience*, *13*. https://www.frontiersin.org/article/10.3389/fncel.2019.00441

Gray, C. M. (1994). Synchronous oscillations in neuronal systems: Mechanisms and functions. *Journal of Computational Neuroscience*, *1*(1), 11–38. https://doi.org/10.1007/BF00962716

Guo, J.-Z., Sauerbrei, B. A., Cohen, J. D., Mischiati, M., Graves, A. R., Pisanello, F., Branson, K. M., & Hantman, A. W. (2021). Disrupting cortico-cerebellar communication impairs dexterity. *ELife*, *10*, e65906. https://doi.org/10.7554/eLife.65906

Hanaie, R., Mohri, I., Kagitani-Shimono, K., Tachibana, M., Azuma, J., Matsuzaki, J., et al. (2013). Altered microstructural connectivity of the superior cerebellar peduncle is related to motor dysfunction in children with autistic spectrum disorders. *Cerebellum* 12, 645–656. doi: 10.1007/s12311-013-0475-x

Hampson, D. R., & Blatt, G. J. (2015). Autism spectrum disorders and neuropathology of the cerebellum. *Frontiers in Neuroscience*, *9*, 420. https://doi.org/10.3389/fnins.2015.00420

Herculano-Houzel, S. (2010). Coordinated scaling of cortical and cerebellar numbers of neurons. *Frontiers in Neuroanatomy*, *4*. https://doi.org/10.3389/fnana.2010.00012

Heuvel, M. P. van den, & Yeo, B. T. T. (2017). A Spotlight on Bridging Microscale and Macroscale Human Brain Architecture. *Neuron*, *93*(6), 1248–1251. https://doi.org/10.1016/j.neuron.2017.02.048

IBM Corp. Released 2021. IBM SPSS Statistics for Windows, Version 28.0. Armonk, NY: IBM Corp

Ingram, J. L., Peckham, S. M., Tisdale, B., & Rodier, P. M. (2000). Prenatal exposure of rats to valproic acid reproduces the cerebellar anomalies associated with autism. *Neurotoxicology and Teratology*, *22*(3), 319–324. https://doi.org/10.1016/s0892-0362(99)00083-5

Johannessen, C. U., & Johannessen, S. I. (2003). Valproate: Past , Present , and Future

Mechanisms of Action. *CNS Drug Reviews*, *9*(2), 199–216.
Jung, G., Yoon, J., Moon, B., Yang, D., Kim, H., Lee, S., Bryja, V., Arenas, E., & Choi, Y. (2008). *in neural progenitor cells via the beta-catenin-Ras-ERK-p21 Cip / WAF1 pathway*. *12*, 1–12. https://doi.org/10.1186/1471-2121-9-66
Just, M. A., Cherkassky, V. L., Keller, T. A., Kana, R. K., & Minshew, N. J. (2007). Functional and anatomical cortical underconnectivity in autism: Evidence from an fMRI study of an executive function task and corpus callosum morphometry. *Cerebral Cortex*, *17*(4), 951–961. https://doi.org/10.1093/cercor/bhl006.Functional
Just, M. A., Cherkassky, V. L., Keller, T. A., & Minshew, N. J. (2004). Cortical activation and synchronization during sentence comprehension in high-functioning autism: Evidence of underconnectivity. *Brain*, *127*(8), 1811–1821. https://doi.org/10.1093/brain/awh199
Kataoka, S., Takuma, K., Hara, Y., Maeda, Y., & Ago, Y. (2013). Autism-like behaviours with transient histone hyperacetylation in mice treated prenatally with valproic acid. *Neuropsychopharmacology*, *16*, 91–103. https://doi.org/10.1017/S1461145711001714
Kaur, M., M Srinivasan, S., & N Bhat, A. (2018). Comparing motor performance, praxis, coordination, and interpersonal synchrony between children with and without Autism Spectrum Disorder (ASD). *Research in developmental disabilities*, *72*, 79–95. https://doi.org/10.1016/j.ridd.2017.10.025
Khambhati, A. N., Sizemore, A. E., Betzel, R. F., & Bassett, D. S. (2018). Modeling and interpreting mesoscale network dynamics. *NeuroImage*, *180*, 337–349. https://doi.org/10.1016/j.neuroimage.2017.06.029
Kim, J. E., Shin, M. S., Seo, T. B., Ji, E. S., Baek, S. S., Lee, S. J., et al. (2013). Treadmill exercise ameliorates motor disturbance through inhibition of apoptosis in the cerebellum of valproic acid-induced autistic rat pups. *Mol. Med. Rep.* 8, 327–334. doi: 10.3892/mmr.2013.1518
Kim, K. C., Lee, D., Go, H. S., Kim, P., Choi, C. S., & Kim, J. (2014). *Pax6-Dependent Cortical Glutamatergic Neuronal Differentiation Regulates Autism-Like Behavior in Prenatally Valproic Acid-Exposed Rat Offspring*. 512–528. https://doi.org/10.1007/s12035-013-8535-2
Landrigan, P. J. (2010). What causes autism? Exploring the environmental contribution. *Current Opinion in Pediatrics*, *22*(2), 219–225. https://doi.org/10.1097/MOP.0b013e328336eb9a
MathWorks, Inc. (1996). MATLAB: the language of technical computing: computation, visualization, programming: installation guide for UNIX version 5. Natwick: Math Works Inc.
Minshew, N. J., & Keller, T. A. (2010). The nature of brain dysfunction in autism: Functional brain imaging studies. *Current Opinion in Neurology*, *23*(2), 124–130. https://doi.org/10.1097/WCO.0b013e32833782d4
Moore, S. J., Turnpenny, P., Quinn, A., Glover, S., Lloyd, D. J., Montgomery, T., & Dean, J. C. (2000). A clinical study of 57 children with fetal anticonvulsant syndromes. *Journal of Medical Genetics*, *37*(7), 489–497. https://doi.org/10.1136/jmg.37.7.489
Mowery, T. M., Wilson, S. M., Kostylev, P. V., Dina, B., Buchholz, J. B., Prieto, A. L., & Garraghty, P. E. (2015). Embryological exposure to valproic acid disrupts morphology of the deep cerebellar nuclei in a sexually dimorphic way. *International Journal of Developmental Neuroscience: The Official Journal of the International Society for Developmental Neuroscience*, *40*, 15–23. https://doi.org/10.1016/j.ijdevneu.2014.10.003

Nicolini, C., & Fahnestock, M. (2018). The valproic acid-induced rodent model of autism. *Experimental Neurology*, *299*(Pt A), 217–227. https://doi.org/10.1016/j.expneurol.2017.04.017

Nguyen VT, Sonkusare S, Stadler J, Hu X, Breakspear M, Guo CC. Distinct cerebellar contributions to cognitive-perceptual dynamics during natural viewing. Cereb Cortex 2017; 27:5652–5662.

O'Reilly, J. X., Beckmann, C. F., Tomassini, V., Ramnani, N., & Johansen-Berg, H. (2010). Distinct and Overlapping Functional Zones in the Cerebellum Defined by Resting State Functional Connectivity. *Cerebral Cortex (New York, NY)*, *20*(4), 953–965. https://doi.org/10.1093/cercor/bhp157

Ozonoff, S., Iosif, A.-M., Baguio, F., Cook, I. C., Hill, M. M., Hutman, T., Rogers, S. J., Rozga, A., Sangha, S., Sigman, M., Steinfeld, M. B., & Young, G. S. (2010). A Prospective Study of the Emergence of Early Behavioral Signs of Autism. *Journal of the American Academy of Child and Adolescent Psychiatry*, *49*(3), 256-66.e1-2.

Palesi, F., Lorenzi, R.M., Casellato, C., Ritter, P., Jirsa, V., Gandini Wheeler-Kingshott, C.A.M., and D'Angelo, E. (2020) The Importance of Cerebellar Connectivity on Simulated Brain Dynamics. *Front. Cell. Neurosci.* 14:240. doi: 10.3389/fncel.2020.00240

Palesi, F., De Rinaldis, A., Castellazzi, G. *et al.* Contralateral cortico-ponto-cerebellar pathways reconstruction in humans *in vivo*: implications for reciprocal cerebro-cerebellar structural connectivity in motor and non-motor areas (2017). *Scientific Reports,* **7(1),** 12841. https://doi.org/10.1038/s41598-017-13079-8

Paxinos, G. and Watson, C. (2013). The Rat Brain in Stereotaxic Coordinates (7th Edition)

Pierpaoli, C., Barnett, A., Pajevic, S., Chen, R., Penix, L., Virta, A., & Basser, P. (2001). Water Diffusion Changes in Wallerian Degeneration and Their Dependence on White Matter Architecture. *NeuroImage*, *13*(6), 1174–1185. https://doi.org/10.1006/nimg.2001.0765

Phiel, C. J., Zhang, F., Huang, E. Y., Guenther, M. G., Lazar, M. A., & Klein, P. S. (2001). Histone Deacetylase Is a Direct Target of Valproic Acid , a Potent Anticonvulsant , Mood Stabilizer , and Teratogen *. *The Journal of Biological Chemistry*, *276*(39), 36734–36741. https://doi.org/10.1074/jbc.M101287200

Purves, D., Augustine, G. J., Fitzpatrick, D., Katz, L. C., LaMantia, A.-S., McNamara, J. O., & Williams, S. M. (2001). Circuits within the Cerebellum. *Neuroscience. 2nd Edition*. https://www.ncbi.nlm.nih.gov/books/NBK10865/

Rodier, Patricia M. (2002). Converging evidence for brain stem injury in autism. *Development and Psychopathology*, *14*(3), 537–557. https://doi.org/10.1017/s0954579402003085

Rogers, T. D., McKimm, E., Dickson, P. E., Goldowitz, D., Blaha, C. D., & Mittleman, G. (2013). Is autism a disease of the cerebellum? An integration of clinical and pre-clinical research. *Frontiers in Systems Neuroscience*, *7*, 15. https://doi.org/10.3389/fnsys.2013.00015

Roullet, F. I., Wollaston, L., Decatanzaro, D., & Foster, J. A. (2010). Behavioral and molecular changes in the mouse in response to prenatal exposure to the anti-epileptic drug valproic acid. *Neuroscience*, *170*(2), 514–522. https://doi.org/10.1016/j.neuroscience.2010.06.069

Roux, S., Bailly, Y., & Bossu, J. L. (2019). Regional and sex-dependent alterations in Purkinje cell density in the valproate mouse model of autism. *Neuroreport*, *30*(2), 82–88. https://doi.org/10.1097/WNR.0000000000001164

Sasson, N. J., Lam, K. S., Parlier, M., Daniels, J. L., & Piven, J. (2013). Autism and the broad autism phenotype: Familial patterns and intergenerational transmission. *Journal of Neurodevelopmental Disorders*, *5*(1), 11. https://doi.org/10.1186/1866-1955-5-11

Schindelin, J., Arganda-Carreras, I., Frise, E., Kaynig, V., Longair, M., Pietzsch, T., … Cardona, A. (2012). Fiji: an open-source platform for biological-image analysis. *Nature Methods*, *9*(7), 676–682. doi:10.1038/nmeth.2019

Schumann, C. M., & Nordahl, C. W. (2011). Bridging the Gap between MRI and Postmortem Research in Autism. *Brain Research*, *1380*, 175–186. https://doi.org/10.1016/j.brainres.2010.09.061.Bridging

Schmahmann, J. D., & Sherman, J. C. (1998). The cerebellar cognitive affective syndrome. *Brain: A Journal of Neurology*, *121 (Pt 4)*, 561–579. https://doi.org/10.1093/brain/121.4.561

Schneider, T., & Przewłocki, R. (2005). Behavioral Alterations in Rats Prenatally Exposed to Valproic Acid: Animal Model of Autism. *Neuropsychopharmacology*, *30*(1), 80–89. https://doi.org/10.1038/sj.npp.1300518

Shepherd, GM (1994). Neurobiology (3rd Ed), New York, NY, Oxford University Press.

Skefos, J., Cummings, C., Enzer, K., Holiday, J., Weed, K., Levy, E., Yuce, T., Kemper, T., & Bauman, M. (2014). Regional Alterations in Purkinje Cell Density in Patients with Autism. *PLoS ONE*, *9*(2), e81255. https://doi.org/10.1371/journal.pone.0081255

Spaeth, L., Bahuguna, J., Gagneux, T., Dorgans, K., Sugihara, I., Poulain, B., Battaglia, D., & Isope, P. (2022). Cerebellar connectivity maps embody individual adaptive behavior in mice. *Nature Communications*, *13*(1), 580. https://doi.org/10.1038/s41467-022-27984-8

Sporns, O. Connectome Networks: From Cells to Systems (2016). In: Kennedy H, Van Essen DC, Christen Y, editors. Micro-, Meso- and Macro-Connectomics of the Brain [Internet]. Cham (CH): Springer; 2016. Available from: https://www.ncbi.nlm.nih.gov/books/NBK435773/doi: 10.1007/978-3-319-27777-6_8

Stoodley, C. J., D'Mello, A. M., Ellegood, J., Jakkamsetti, V., Liu, P., Nebel, M. B., Gibson, J. M., Kelly, E., Meng, F., Cano, C. A., Pascual, J. M., Mostofsky, S. H., Lerch, J. P., & Tsai, P. T. (2017). Altered cerebellar connectivity in autism spectrum disorders and rescue of autism-related behaviors in mice. *Nature Neuroscience*, *20*(12), 1744–1751. https://doi.org/10.1038/s41593-017-0004-1

Thoma, P., Bellebaum, C., Koch, B., Schwarz, M., & Daum, I. (2008). The cerebellum is involved in reward-based reversal learning. *Cerebellum*, *7*(3), 433–443. https://doi.org/10.1007/s12311-008-0046-8

Varghese M, Keshav N, Jacot-Descombes S, Warda T, Wicinski B, Dickstein DL, Harony-Nicolas H, De Rubeis S, Drapeau E, Buxbaum JD, Hof PR. (2017). Autism spectrum disorder: neuropathology and animal models. *Acta Neuropathol*, 134(4):537-566. doi: 10.1007/s00401-017-1736-4.

Wang, R., Tan, J., Guo, J., Zheng, Y., Han, Q., So, K.-F., Yu, J., & Zhang, L. (2018). Aberrant Development and Synaptic Transmission of Cerebellar Cortex in a VPA Induced Mouse Autism Model. *Frontiers in Cellular Neuroscience*, *12*. https://doi.org/10.3389/fncel.2018.00500

Wang, S. S.-H., Kloth, A. D., & Badura, A. (2014). The Cerebellum, Sensitive Periods, and Autism. *Neuron*, *83*(3), 518–532. https://doi.org/10.1016/j.neuron.2014.07.016

Weston C. (2019). Four Social Brain Regions, Their Dysfunctions, and Sequelae, Extensively

Explain Autism Spectrum Disorder Symptomatology. *Brain Sciences*, *9* (6), 130. https://doi.org/10.3390/brainsci9060130

Whitney, E. R., Kemper, T. L., Rosene, D. L., Bauman, M. L., & Blatt, G. J. (2009). Density of cerebellar basket and stellate cells in autism: Evidence for a late developmental loss of Purkinje cells. *Journal of Neuroscience Research*, *87*(10), 2245–2254. https://doi.org/10.1002/jnr.22056

Yochum, C. L., Dowling, P., Reuhl, K. R., Wagner, G. C., & Ming, X. (2008). VPA-induced apoptosis and behavioral deficits in neonatal mice. *Brain Research*, *1203*, 126–132. https://doi.org/10.1016/j.brainres.2008.01.055

Zeng H. (2018). Mesoscale connectomics. *Curr Opin Neurobiol*. 50:154-162. doi: 10.1016/j.conb.2018.03.003.

Appendices (AP)

(A)

Tests of Between-Subjects Effects (Dependent Variable: PC Count - Hemisphere)		
Source	F-value	P-value
Lobules of the Hemisphere	54.357	<0.001
Group	29.446	<0.001
Lobules of the Hemisphere * Group Interaction	1.566	0.189

Pairwise Comparison (Dependent Variable: PC Count - Hemisphere)				
Cerebellar Lobules of Hemisphere	Group (1)	Group (2)	Mean Difference	P-value
COP	CTRL	VPA	32.541	0.225
CrusI	CTRL	VPA	10.971	0.164
CrusII	CTRL	VPA	33.126*	0.003
PM	CTRL	VPA	33.126*	<0.001
Simplex	CTRL	VPA	37.405*	0.026

(B)

Tests of Between-Subjects Effects (Dependent Variable: PC linear density - Hemisphere)		
Source	F-value	P-value
Lobules of the Hemisphere	52.272	0.06
Group	36.589	<0.001
Lobules of the Hemisphere * Group Interaction	0.601	0.657

Pairwise Comparison (Dependent Variable: PC linear density - Hemisphere)				
Lobules of Cerebellar Hemisphere	Group (1)	Group (2)	Mean Difference	P-value
COP	CTRL	VPA	7.362*	<0.001
CrusI	CTRL	VPA	4.299*	0.025
CrusII	CTRL	VPA	6.22*	0.003
PM	CTRL	VPA	6.402*	0.002
Simplex	CTRL	VPA	3.401	0.14

(C)

Tests of Between-Subjects Effects (Dependent Variable: PC Count -Vermis)		
Source	F-value	P-value
Group	0.423	0.519
Lobules of the Vermis	2.695	0.078
Lobules of the Vermis * Group Interaction	1.061	0.354

Pairwise Comparison (Dependent Variable: PC Count - Vermis)				
Lobules of the Vermis	Group (1)	Group (2)	Mean Difference	P-value
Lobule 6	CTRL	VPA	111.962*	0.026
Lobule 7-8-9	CTRL	VPA	53.3	0.278
Lobule 10	CTRL	VPA	-71.8	0.573

(D)

Tests of Between-Subjects Effects (Dependent Variable: PC Linear Density - Vermis)		
Source	F-value	P-value
Group	0.168	0.684
Lobules of the Vermis	0.235	0.792
Lobules of the Vermis * Group Interaction	1.093	0.344

Pairwise Comparison (Dependent Variable: PC Linear Density - Vermis)				
Lobules of the Vermis	Group (1)	Group (2)	Mean Difference	P-value
Lobule 6	CTRL	VPA	-1.158	0.79
Lobule 7-8-9	CTRL	VPA	5.474	0.212
Lobule 10	CTRL	VPA	-9.571	0.4

Table AP1: Test of Between-Subjects Effects and Pairwise Comparison of PC count and linear density in the lobules of cerebellar hemisphere (A, B) and vermis (C, D) in the control and VPA-exposed groups (Two-way ANOVA, SPSS). (A) Tables showing data of the PC count in the tests of Between-Subjects Effects and the pairwise comparison of the two-ANOVA. The two independent variables: (1) lobules of the hemisphere and (2) group on PC count. The tests of Between-Subjects Effects table measure the effect of each of the variables as well as their interaction and includes the F-value and P-value of each. The pairwise comparison table shows the mean difference and the P-value of the PC count in each of the lobules of the hemisphere between the Control and VPA groups. The cerebellar lobules of the hemisphere include the Simplex, Crus I, Crus II, Paramedian (PM), and Copula pyramidis (Cop). All these values are retracted from the two-way ANOVA test that was performed in SPSS. (B) same tables as (A) for the linear density measurement. Tables C, and D are similar tables as A and B for the lobules of the cerebellar vermis. The significance threshold was set at $p<0.05$. Based on estimated marginal means, the star (*) is the significant mean difference at the 0.05 level. All values highlighted in light gray show significant p-values.

(A)

Descriptive Statistics (Dependent Variable: DCN Cell Count and within-area density of DCN)		
Nucleus	**Group**	**Sample size (N)**
Intermediate	CTRL	4
	VPA	7
	Total	11
Medial	CTRL	7
	VPA	18
	Total	25
Total	CTRL	11
	VPA	25
	Total	36

(B)

Tests of Between-Subjects Effects (DCN Cell Count)		
Source	F-value	P-value
DCN Cell	40.33	<0.001
Group	12.174	0.001
DCN Cell * Group Interaction	4.08	0.052

Pairwise Comparison (DCN Cell Count)				
Nucleus	Group (1)	Group (2)	Mean Difference	P-value
Intermediate	CTRL	VPA	-153.964*	0.002
Medial	CTRL	VPA	-41.063	0.214

(C)

Tests of Between-Subjects Effects (Within-Area Density of DCN Cell)		
Source	F-value	P-value
DCN Cell	1.685	0.204
Group	2.958	0.095
DCN Cell * Group Interaction	0.546	0.465

Pairwise Comparison (Within-Area Density of DCN Cell)				
Nucleus	Group (1)	Group (2)	Mean Difference	P-value
Intermediate	CTRL	VPA	-508.107	0.551
Medial	CTRL	VPA	-1273.034*	0.042

Table AP2: Descriptive analysis and pairwise comparison of DCN cell counts and within-area density of DCN cells in intermediate and medial DCN sectors in control and VPA-exposed rats. (A) Descriptive statistics of the DCN cell count and within-area density of DCN cells in control and VPA-exposed rats. Measurements include the mean, the standard deviation, and the sample sizes. The nuclei include the intermediate and medial cells. (B) Tables showing data of the DCN cell count in the tests of Between-Subjects Effects and the pairwise comparison of the two-ANOVA. The two independent variables measured are: (1) DCN cell (Intermediate and Medial) and (2) Group (Control and VPA). The tests of Between-Subjects Effects table measure the effect of each of the variables as well as their interaction and includes the F-value and P-value of each. The pairwise comparison table shows the mean difference and the P-value of the DCN cell count in each of the DCN cells between Control and VPA groups. (C) same tables as (B) for the within-area density of the DCN cells. The significance threshold was set at $p<0.05$. Based on estimated marginal means, the star (*) is the significant mean difference at the 0.05 level. All values highlighted in light gray show significant p-values.

Descriptive and Test Statistics of GCL Thickness measurements						
Cerebellar Lobules			Group	Mean Rank of GCL Thickness (in μm)	Kruskal-Wallis H	P-value
Cerebellar Lobules	Hemisphere	Simplex	CTRL	57.48	0.009	0.923
			VPA	56.82		
		Crus I	CTRL	226.90	0.340	0.560
			VPA	219.78		
		Crus II	CTRL	271.41	0.392	0.531
			VPA	263.04		
		PM	CTRL	170.47	0.157	0.692
			VPA	166.25		
		Cop	CTRL	104.42	1.285	0.257
			VPA	94.79		
	Vermis	Lobule 6	CTRL	214.32	27.454	<0.001
			VPA	**156.05**		
		Lobule 7-8-9	CTRL	168.84	6.854	0.009
			VPA	**198.19**		
		Lobule 10	CTRL	12.84	23.106	<0.001
			VPA	**33.26**		
Combined Lobules of the Vermis and Hemisphere			CTRL	1219	1.062	0.302
			VPA	**1187**		

Table AP3: Descriptive and Test Statistics of GCL Thickness measurements in the combined lobules and specific lobules of the cerebellar hemisphere and the vermis in Control and VPA groups. All values in this table are retracted from the Kruskal-Wallis test for the GCL thickness measurements. The table reports the mean rank of GCL thickness (in μm) in each group (CTRL and VPA) of each lobule from the hemisphere and vermis as well as the combined lobules of the cerebellum. The Kruskal-Wallis H and p-value are also reported for the difference in GCL thickness distribution between the two groups in the lobules. The lobules of the cerebellar hemisphere include the Simplex, Crus I, Crus II, PM, and Cop while the lobules of the cerebellar vermis include Lobule 6, Lobule 7-8-9, and Lobule 10. The combined lobule of the cerebellum includes all the lobules of the cerebellar hemisphere and vermis. All values highlighted in light gray show significant p-values. CTRL = control group and VPA = VPA-exposed rats.